Seismic Damage Avoidance Design of Moment Resisting Frames Using a New Self-Centring Friction Connection System

Seyedmohsen Shabankareh

A thesis submitted to Auckland University of Technology in fulfilment of the requirements for the degree of Master of Engineering

Primary Supervisor: Dr Pouyan Zarnani

Department of Built Environment Engineering
New Zealand

October 2020

Abstract

Moment-resisting frames are one of the efficient lateral-load resisting systems in terms of providing architectural freedom in design and widely distributing the seismic forces within the structure and into the foundation. Recent major earthquakes have resulted in significant plastic deformations in the beams, columns and connections causing irrecoverable damage in structures. As a result, engineers have focused on developing new systems which not only provide the life-safety of the residents, but also minimise the damage such that the building could be reoccupied quickly after severe events with minimal business interruption and repair costs.

In this research, a self-centring damage avoidance concept using an innovative Resilient Slip Friction Joint (RSFJ) is developed for steel Moment Resisting Frames (MRFs). The RSFJ provides the self-centring behaviour as well as energy dissipation in one compact component requiring no post-event maintenance. In this concept, the beam is connected to the column using a pin assembly at top, and the RSFJs acting in tension and compression at the beam bottom. The RSFJs allow for the gap opening in the connection during loading and re-centre the system upon unloading. Furthermore, a secondary collapse-prevention fuse within the RSFJ is considered to keep maintaining a ductile behaviour in the system in case of an event greater than the design earthquake.

In this research an analytical model was developed to accurately predict the moment-rotation behaviour of this system. The seismic performance of the proposed concept was investigated by a full-scale beam-end connection test. The tests results validate the predictive model and demonstrate the efficiency of this new self-centring system for seismic damage avoidance design of MRFs.

Table of contents

Attestation of Authorship

I hereby declare that this submission is my own work and that, to the best of my knowledge and belief, it contains no material previously published or written by another person, nor material which to a substantial extent has been submitted for the award of any other degree or diploma of a university or other institution of higher learning.

List of Figures

List of Tables

1. Introduction

In the 1994 Northridge and 1995 Kobe earthquakes, many conventional moment welded steel connections suffered from premature brittle fractures in the beam flange to column flange welds and in some cases in the column flange to beam web connections. While in many cases connection failures did not cause the collapse of buildings in Northridge, they led to significant damage to the structures resulting in a considerable economic impact. The extent of earthquake damage in Kobe was much more noteworthy, with more than 50 steel structures collapsing, confirming the potential vulnerability of steel structures through their connection failure. Alternative methods and procedures have since been developed to avoid weld failure in steel connections.

These strategies like the reduced beam section and bolted flange plate connections (Roeder, 2002) are typically based on capacity design principles, where energy is dissipated through controlled damage in designated plastic hinge zones, thereby protecting the integrity of the joints and structural system. In steel moment resisting frames (MRFs), this includes forcing plastic hinges to make in the beam away from face of the column to dissipate energy without affecting the structural integrity of the building in a weak beam strong column system.

Although these systems are effective to provide safety and prevent collapse, they are usually associated with irrecoverable plastic deformation in the beams or joints. This could lead to significant economic losses in both post-disaster repairs (direct costs), and downtime due to closure of the building (indirect costs). The indirect costs while often ignored are significant and may escalate the direct costs related with the physical damage causes by the earthquake (Comerio, 2006).

The economy of a society can be severely disrupted with long term impacts, especially in highly developed regions. Damage can cause people to leave their home and constrain businesses to

close. The 1994 Northridge earthquake caused more than USD 20 billion in property damage alone, and a further USD 6 billion in commerce interruption (Tierney, 1997). While relatively few lives were lost, it has been the costliest earthquake in the United States history, with a considerable long-term economic impact. The 1999 Taiwan earthquake claimed 2,500 lives and left more than 10,000 people homeless, costing USD 11.5 billion (Yeh et al., 2006). The 1995 Kobe earthquake caused only an estimated USD 114 billion in direct damage, which was 2.3% of Japan's overall gross domestic product (GDP) of Japan (Horwich, 2000), not including long lasting effects. In spite of rebuilding, Kobe the sixth largest port in the world, suffered noteworthy permanent loss in container traffic to other ports (Chang and Falit-Baiamonte, 2002).

Following the 2010 and 2011 Christchurch earthquake sequence, it is estimated that the repair and replacement of buildings and infrastructure alone will cost NZD 20 billion (New Zealand Treasury, 2012), which corresponds to around 10% of New Zealand's GDP (IMF estimate). In response to the adverse financial consequences of earthquakes, there has been interest in the development and implementation of low damage seismic systems. The objective is to not only avoid building from collapse, but also to enable rapid or ideally, prompt return to occupancy after a severe earthquake. Any minor damage that may happen could be repaired easily and inexpensively.

A number of low damage alternatives to plastic beam hinging in steel MRFs have been developed to minimise permanent deformation and residual drifts in buildings as a result of earthquake shaking. These involve beam end connections providing non-linear resistance to dissipate the energy with negligible damage, while the structural members stay elastic. The main objective of the current research is to introduce a new damage free connection system for MRFs to provide damping as well as full self-centring with no post-event maintenance allowing for quick reoccupancy and having buildings which could withstand aftershocks.

2. Literature Review

This section provides an overview of the research related to steel MRF connection systems. It covers the conventional moment connections, connections with yieldable fuses, post-tensioned steel tendon systems and sliding hinge connections.

2.1. Moment connections

Conventional moment beam-column connections are designed with a philosophy of strong column-strong connection-weak beam. Illustrations of moment connections include BFP (Bolted Flange Plate) connections, WUF-W (Welded Unreinforced Flange-Welded Web) connections, and more recently RBS (Reduced Beam Section) Connections. Schematics of typical connections are shown in Figure 2-1. The aim of conventional moment connections is to force inelastic action to occur in the beams adjacent to (away from) the connections.

Moment connections if well designed and detailed, are able to undergo large plastic rotations while maintaining their integrity. The behaviour has been shown experimentally through testing of various moment connection types. In order to provide ductility, the connections are designed to ensure a yield mechanism of flexural yielding of the beam or tensile yielding in the flange plates, while suppressing other failure modes. While other failure modes such as web and/or flange buckling, lateral torsional buckling and excessive plastic deformation of the beam and/or column do provide a reasonable amount of ductility, bolt shear fracture and weld fracture can result in undesirable brittle failure modes (Roeder, 2002). These failure modes are suppressed through good detailing and capacity design of the respective components. However, suppression of these failure modes can result in large component sizes (eg. columns) as the connections tend to develop much larger failure strengths than the yield moment due to material strain hardening. While the enhancement of joint strength improves the seismic response of buildings and provides stability, it also increases the demand in the column and welds.

The design of moment frames is also often governed by the frame lateral stiffness, requiring large beam sizes to control drift. As the joint strength is dependent on the beam size, large demands are transferred to the column. The connection must be sufficiently strong to develop the overstrength demands from the beam to prevent concentration of the inelastic behaviour in the connection. More recently, RBS connections have been developed, which create a fuse in the beam where yielding occurs to control the column failure and to protect the components in the connection (Roeder, 2002). The RBS allows a greater control of the demands in the column and weld. The increase in strength due to strain hardening is also reduced in RBS connections, but also causes a higher potential of lateral instability. However, while these systems achieve good performance with regards to collapse prevention and life safety, their ductile behaviour is associated with permanent deformation in the beams. Figures 2-2 and 2-3 show an example of the failure mechanism of a typical WUF-W connection. The irrecoverable plastic deformation in the beams may require replacement of the entire beam or at least a section of it, which would be costly in post-disaster repair.

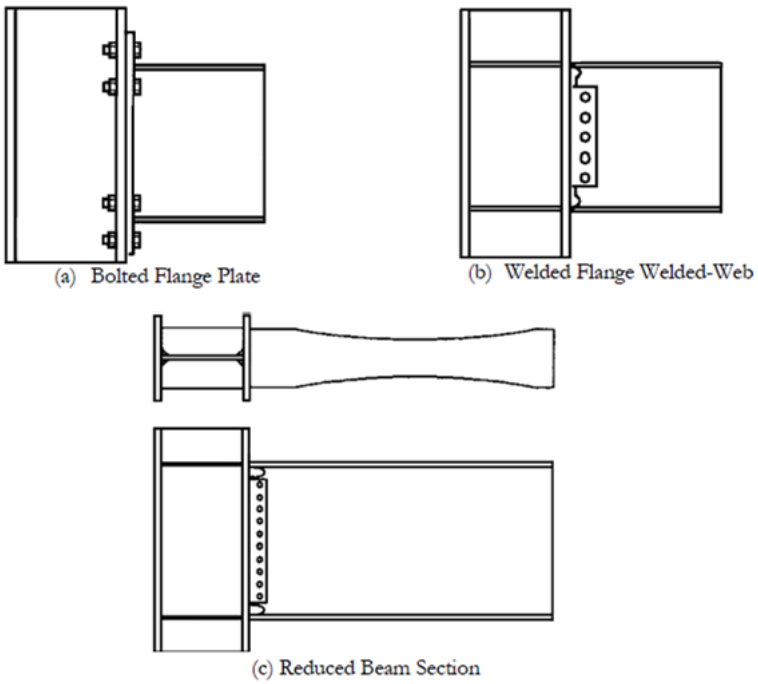

Fig 2-1. Schematic of traditional moment beam-column connection (Roeder, 2002)

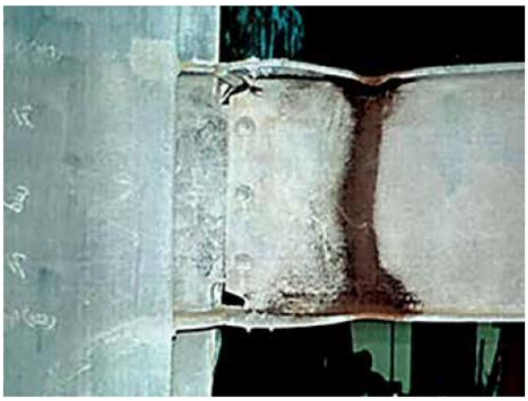

Fig 2-2. Formation of plastic hinge at RBS connection (Gilton, Chi and Uang, UCSD SSRP-2000/03)

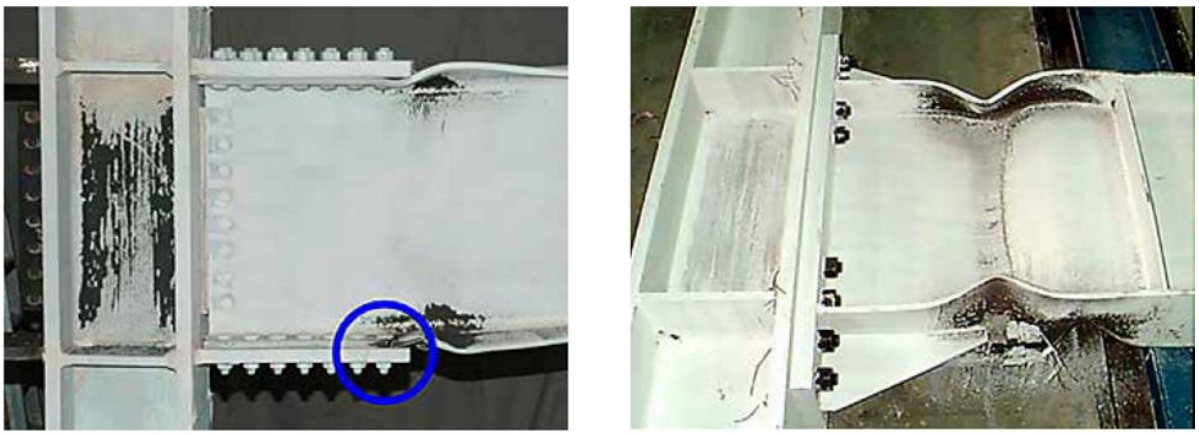

Fig 2-3. Fracture of beam flange plate of a moment connection (Sato, Newell and Uang, UCSD SSRP-2007) (Left); End plate specimen at failure (Sumner et al., 2000) (Right)

2.2. Connections with yieldable fuses

Traditional prequalified moment frames most often require a welded connection with either a weakened beam or a stiffened connection in order to allow the beam to yield as being necessary during a seismic event to dissipate the energy. For these types of connections, as per code requirements, the beam should be braced to resist the lateral torsional buckling.

In this concept, the yielding during a seismic event has been moved from the beams to the Yield-Links (e.g., dog-boned plates), and the connection follows a capacity-based design approach. This allows the connection to remain elastic under factored load combinations, and

the seismic inelastic rotation demand is confined within the connection. With the yielding confined predominantly to the replaceable Yield-Link connection, inelastic behaviour is not expected from the members and no lateral beam buckling braces are required.

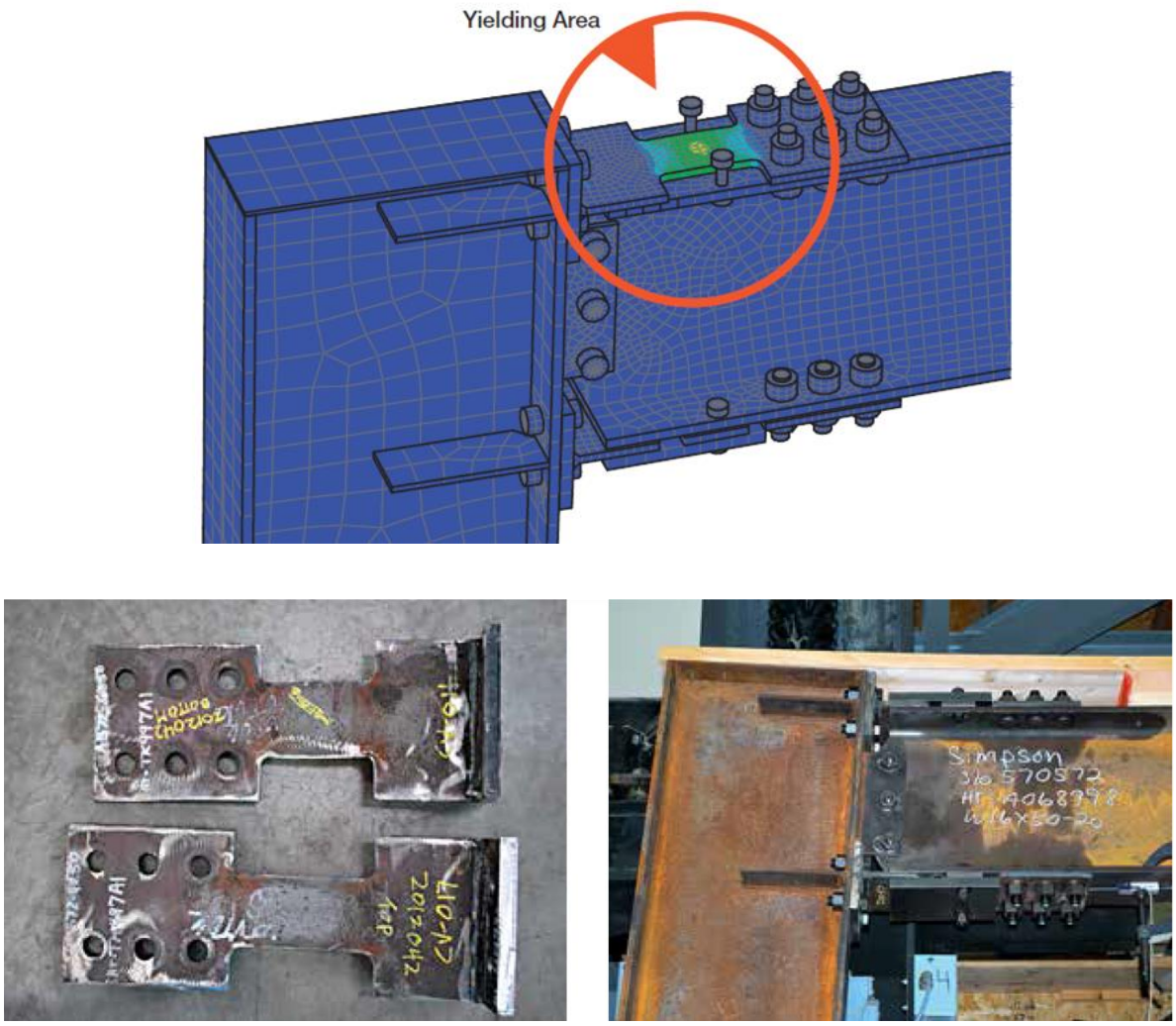

Fig 2-4. Yielding in strong frame links (Simpson Strong-Tie company INC, 2017)

2.3. Post-tensioned systems (with & without damping joints)

Post-tensioned (PT) steel tendon systems have more recently been developed to provide low damage ductility and self-centring characteristics in steel MRFs. (Chou et al., 2008, Christopoulos et al., 2002, Garlock et al., 2005, Iyama et al., 2009, Kim and Christopoulos, 2008, Ricles and Sause, 2001, Wolski et al., 2009)]. These systems involve compressing the beams into the columns with high strength steel tendons that are anchored to the exterior

columns of the frame to develop joint moment capacity. Energy is dissipated through yielding of secondary elements or friction devices. Examples of two proposed connections which incorporate Slotted Bolted Connections (SBCs) to dissipate the energy are shown in Figure 2-5. When the moment in the beams exceeds the resistance provided by the PT strands and energy dissipating devices, the joints rotate inelastically through gap-opening between the beam-column interfaces, resulting in "expansion" of the frame. Upon removal of the applied moment, the tension in the strands closes the gaps between the beam-column interfaces, and thus produces the ideal flag-shaped self-centering hysteresis curves (eg. Figure 2-6) and returns the frame to its original plumb position. Experimental studies have shown that the joints provide stable, repeatable and predictable moment-rotational characteristics.

The joint moment capacity and hysteretic behaviour is however adversely affected by the frame-slab interaction during gap opening. Furthermore, the demand on the frame increases as the floor partially restrains the expansion which may force the inelastic demand beyond the intended ductile elements and also cause significant damage to the slab. To mitigate these effects, Garlock and Li (2008) proposed collector beams to transfer inertia to the frames that are designed to deform. King (2007) and Chou and Chen (2011) proposed connecting the slab to one rigid bay and allowing sliding in the other bays or using a discontinuous slab to allow deformation. These systems were tested showing their effectiveness in isolating the floor slab during inelastic rotation of the joints. However, none of these methods are able to be used easily on large frames without introducing secondary damage.

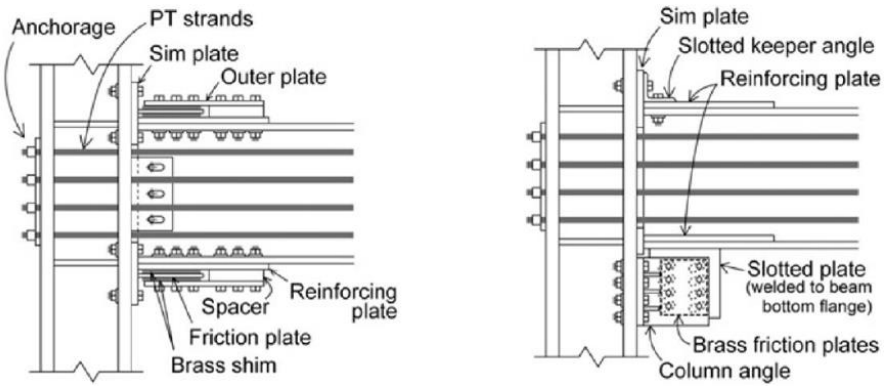

Fig 2-5. PT connection with friction devices (Iyama et al., 2009)

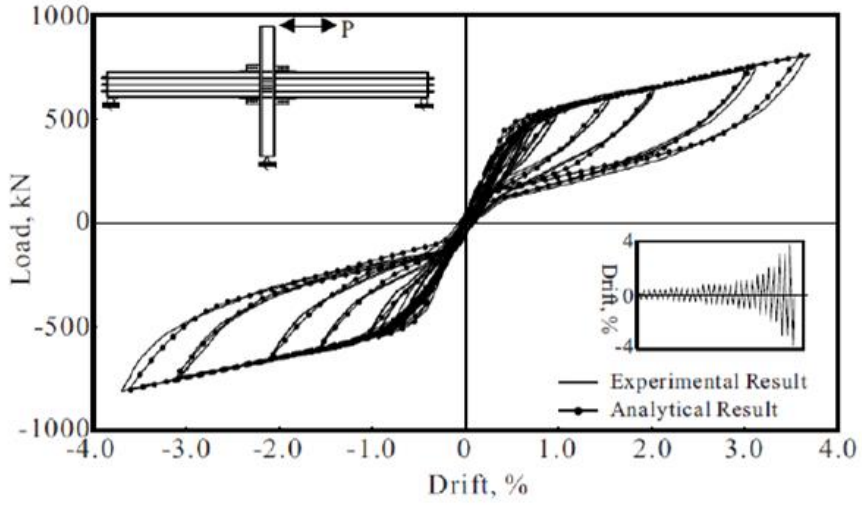

Fig 2-6. Behaviour of PT connection with bottom flange friction device (Kim and Christopoulos, 2008)

Danner and Clifton (1995) studied the feasibility of post-tensioning beams to the columns through a flush endplate connection with conventional post-tensioning bars or with bars incorporating ring springs, replicating the Precast Seismic Structural Systems (PRESSS) used in concrete structures [eg. (Priestley and MacRae, 1996)]. The ring spring option is shown in Figure 2-7.

These systems were characterised by gap-opening at the beam-column interface during large storey drifts, causing damage to the overlaying floor slab. Therefore, they were considered less practical for superstructure beam-column connections. However, they were recommended for use in column bases. As shown in Figure 2-7, ring springs were adopted in the proposed self-

centering moment connection (Clifton, 2005). Ring springs are friction damping springs manufactured by Ringfeder, Germany (Ringfeder Gmbh, 2008). They consist of a set of inner and outer rings with tapered surfaces that slide during deformation and can therefore only be loaded in compression. Their use in seismic applications were also proposed by Filiatrault and colleagues (2000), who tested a dual directional acting seismic damper detailed to compress the ring spring when loaded in both tension and compression, as shown in Figure 2-8. Shake table tests and numerical studies on a single storey braced frame showed that the damper effectively dissipated the energy and reduced the lateral displacements and accelerations. Ring springs have been used in the column base of the Te Puni Village Tower Building at the Victoria University of Wellington in New Zealand (Gledhill et al., 2008) in accordance with the recommendations by Clifton (2005).

Fig 2-7. Ring spring joint (Clifton, 2005)

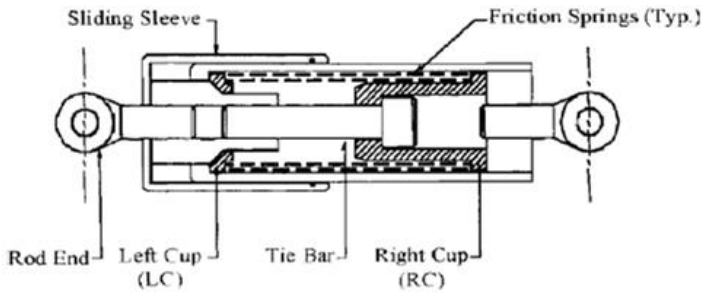

Fig 2-8. Dual direction ring spring seismic damper (Filiatrault et al., 2000)

2.4. Sliding Hinge Joint

The Sliding Hinge Joint (SHJ) was developed by Clifton and colleagues (1998 to 2005) as a low-damage alternative to traditional welded connections. The concept was built on the previous research (Grigorian et al., 1993, Yang and Popov, 1995) on the slotted bolted moment connections. This section describes the development of the SHJ, covering the joint configuration, rotational behaviour and the related experimental and analytical studies. The advantages and limitations of the current system, as well as the limitations on the research undertaken to date are then presented.

The SHJ configuration is presented in Figure 2-9, showing each of the joint components. The beam is connected to the column through the top flange plate, bottom flange plate and web plate. Each of these plates are welded to the column and bolted to the beam. Their description and design rules are summarised as follows:

1. The top flange plate provides a robust connection that pins the top corner of the beam relative to the column, which provides a point of rotation under inelastic rotation and limits the gap opening.

2. The bottom flange bolt group consists of Asymmetric Friction Connections (AFCs). The AFC is a type of slotted bolted connection and a key component of the SHJ that slides while dissipating energy through friction.

3. The bolts in the web plate consist of a standard bolt group in the top web bolts and AFCs in the bottom web bolt group. The top web bolt group is designed to resist joint shear while the bottom web AFC slides during inelastic joint rotation.

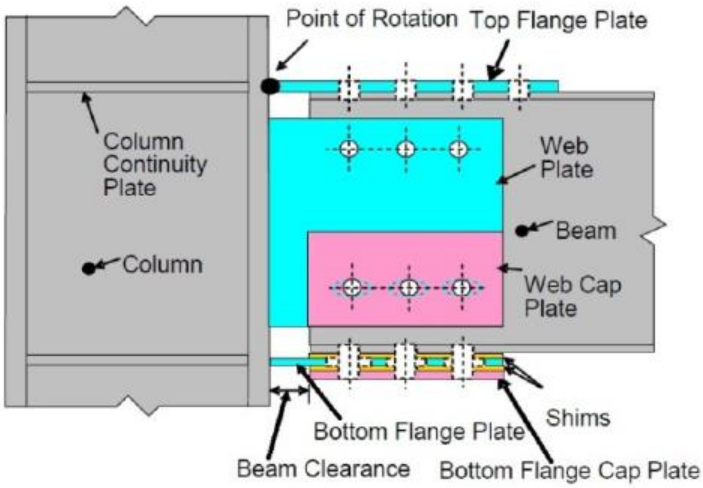

Fig 2-9. Sliding hinge joint layout (Ramhormozian et al., 2014)

The SHJ behaves like a moment connection until the moment in the beam overcomes the frictional resistance provided by the bottom web and bottom flange AFCs. When this occurs, the beam rotates about the top flange plate (relative to the column) through sliding in the AFCs while dissipating energy through friction. The AFCs decouple the joint strength and stiffness, confines the yielding to the bolts, and limits the inelastic demands in the beams and columns (Ramhormozian et al., 2015). Figure 2-10 illustrates the joint rotation under positive and negative moments. The top flange plate was shown experimentally (Clifton, 2005) to not undergo net elongation during inelastic rotation, which limits the beam growth. The testing observation also demonstrated that the rotation about the top flange plate isolates the floor slab, limiting the additional demands to the column and the slab. The slab may be subjected to minor cracking which could be easily repairable. The top flange plate and slab were studied further and the results are reported in this thesis in Chapters 3 and 7, respectively.

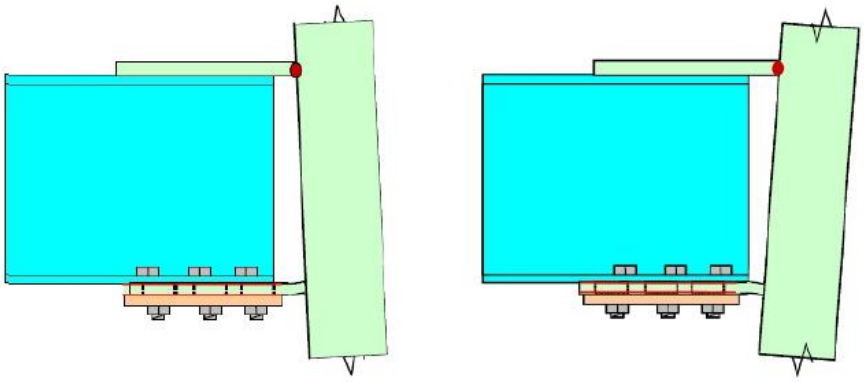

Fig 2-10. Positive and negative rotation of the SHJ (Ramhormozian et al., 2014)

At the onset of sliding, the joint moment-rotational behaviour is dependent on the AFC sliding characteristics. The AFC is a type of slotted bolted connection with a different configuration from the symmetric sliding conditions tested by Grigorian and Popov (1994). The configuration of the AFC in the beam bottom flange is shown in Figure 2-11(a). It consists of five components, namely the beam bottom flange, bottom flange plate (also referred to as the cleat), cap plate, and two shims. The bottom flange plate is sandwiched between the beam bottom flange and the cap plate, with shims in between. Likewise, the web plate AFC consists of the web plate sandwiched by the beam web and cap plate, with shims in between. The bottom flange plate and web plate have elongated holes to allow sliding, with standard sized bolt holes in the beam flange, cap plate and shims. The five plates are bolted with high strength grade class 8.8 bolts, which are fully tensioned at installation (ie. yielded) with the turn-of-nut method in accordance to the New Zealand Steel Structures Standard, NZS 3404 (Standards New Zealand, 2009).

The AFC has two sliding surfaces. The first is the bottom flange/web plate and the upper/inner shim interface, and the second is the bottom flange/web plate and the lower/outer shim plate interface. The rotational behaviour of the SHJ is dependent on the two sliding surfaces of the AFC. The idealised force-displacement behaviour of the AFC is shown in Figure 2-11(b).

When the frictional resistance of one surface is exceeded, the first interface starts to slide, as shown in the force-displacement curve (denoted by B in Figure 2-11). As the demand increases, the cap plate (which acts like a large washer) gets dragged along and the second interface commences sliding, approximately doubling the frictional resistance (denoted by C). When this occurs, the bolts go into double curvature. It then builds up as sliding occurs initially on the first interface (denoted by D) followed by the second interface (denoted by E) as the bolts are pushed into double curvature in the opposite direction. This gives the SHJ a "pinched" hysteretic behaviour. The AFCs are designed to be rigid under the Serviceability Limit State (SLS) level event and slide under the Ultimate Limit State (ULS) design level event. The slotted holes are sized to allow sliding up to 35 milliradians (mrad) rotation, which is above the upper limit expected under the ULS. This is based on the 2.5% inter storey drift limit from the New Zealand Earthquake Design Actions Standard, NZS 1170.5 (Standards New Zealand, 2004), with an "over-rotation factor" of 1.4 applied. Under rare and extreme maximum considered events (MCE), the SHJ would maintain its integrity but undergoes controlled damage as the bolts may hit the end of the slotted holes. The connection then experiences the ductile failure through stretching and yielding in the bottom flange plate. Upon further increases in rotation, the bolts in the bottom flange plate, or the bottom flange plate itself may fracture. The flexural strength in the SHJ would then be carried by the web plate and bolts. This ductile failure mechanism where the joint integrity was maintained was shown experimentally by Clifton (2005), where the SHJ was still able to deliver the design moment capacity at 120 mrads of rotation.

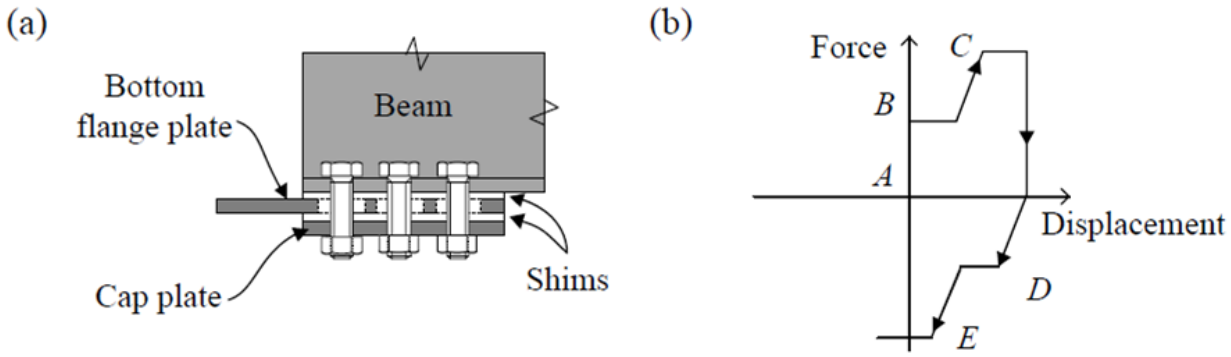

Fig2-11. AFC in the bottom flange plate (Left); and AFC idealised force-displacement behaviour (Right) (Ramhormozian et al., 2014)

3. Resilient Slip Friction Joint (RSFJ)

3.1. Introduction

With a clear worldwide rise in recurrence and effect of severe earthquakes, there is an increasing demand to enhance public safety, limit casualty threats and financial loses in the aftermath of this natural hazard. The impact in the latest major seismic events has led to significant endeavours by engineers to introduce new strategies that not only provide life-safety but also reduce the earthquake destructive impact so that buildings could be reoccupied rapidly with less repair costs and business downtime. There are three important features that are desirable for a structure to be able to withstand the seismic loads with the least damage: 1) damping, 2) self-centring and 3) non-degrading performance.

Typically, dampers can be classified into four diverse categories: 1) friction, 2) metallic, 3) viscoelastic, and 4) viscous. The dynamic behaviour related to each of the dampers mentioned above is characterized by their hysteretic response, as demonstrated in Figure 3-1.

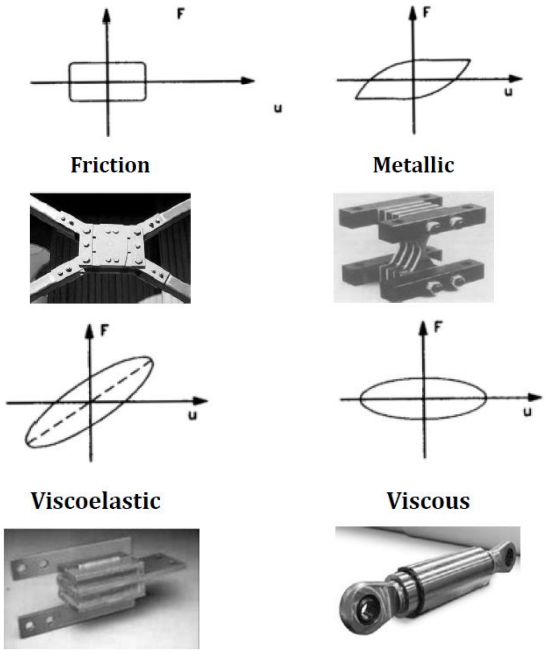

Fig 3-1. Classification of dampers: a) friction, b) metallic, c) viscoelastic, d) viscous (Constantinou and Symans, 1993)

As it can be concluded, none of the energy dissipation systems are thoroughly self-centred after unloading and hence a deformation would be exhibited causing residual drift within the system. As such, an extra self-centring mechanism would be desirable (Figure3-2) to improve the building resilience and avoid post-event maintenance, which is part of the Damage Avoidance Design (DAD) philosophy (Clifton et al., 2012).

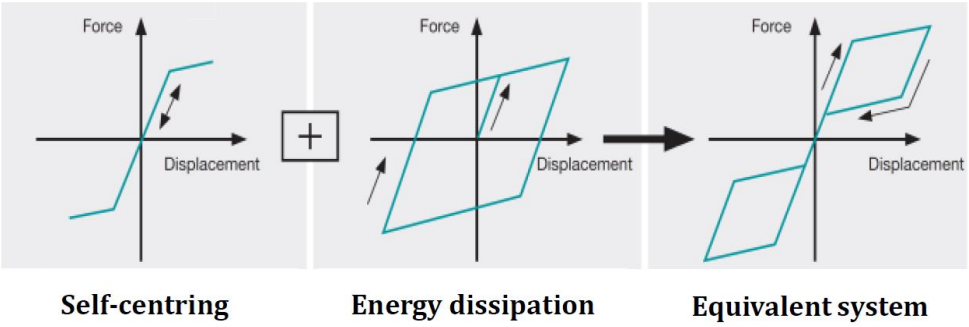

Fig 3-2. Hysteresis response of a system with self-centring and energy dissipating characteristics (CERC, 2012)

Friction joints utilizing simple flat steel plates that slide against each other have already demonstrated to be a viable structural connection solution.

The energy dissipation mechanism of such contact joints is one of the most effective passive devices. However, because these joints do not provide self-centring, additional systems would be needed to restore the structure to its original position after a severe event, which could be expensive. As shown in Figure 3-3, one of the common techniques for self-centring is the application of post-tension tendons.

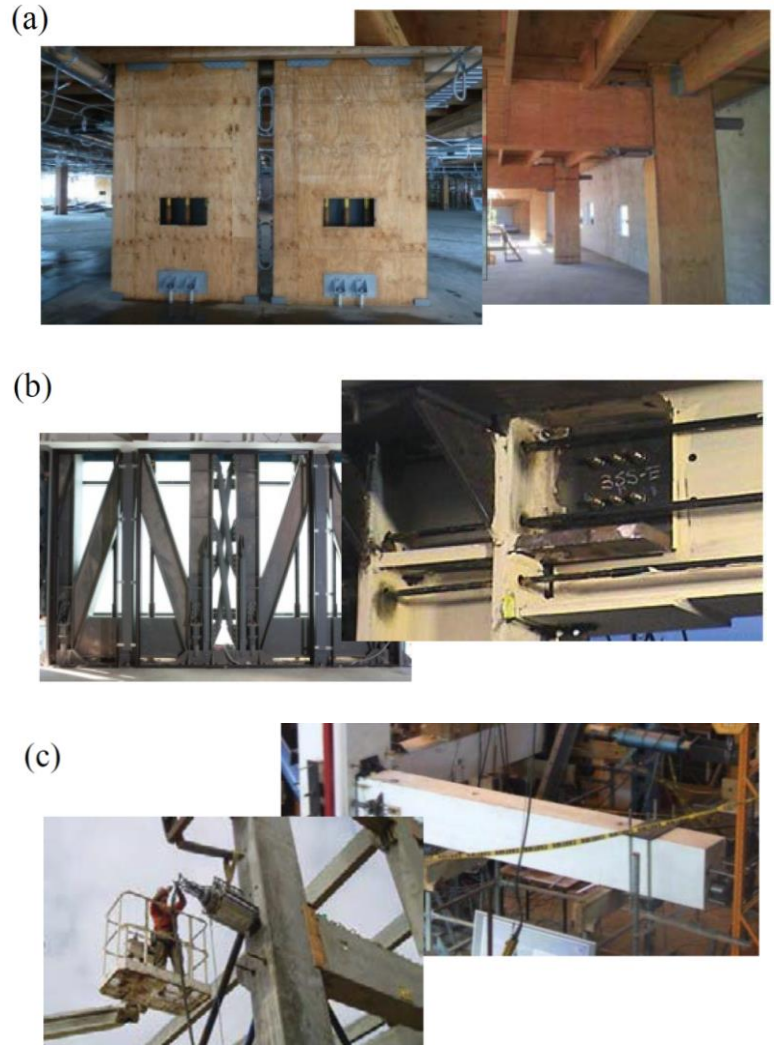

Fig 3-3. Samples of resilient lateral load-resisting systems using post-tensioned tendons: a) Timber structures (Buchanan et al., 2012), b) Steel structures (Build Magazine, 2014), c) Concrete structures (Midstate Precast, L.P., 2012; Rodger et al., 2007)

In this section, a new friction joint is introduced in which the steel parts are groove shaped and discs springs are arranged in such a way to achieve self-centering as well as damping, all in one compact joint system. The new Resilient Slip Friction Joint (RSFJ) developed by Zarnani and Quenneville (2015) could bring some advantages to the building industry given it is in line with the growing need for cost-efficient damage prevention methods, specifically, in high seismic regions such as NZ. This new connection system can

be adopted for new and retrofitted buildings (from low-rise to high-rise) made of timber, steel, concrete or hybrid of any.

3.2. Design considerations and behaviour

Figure 3-4 shows the RSFJ components and its assemblage (Hashemi et al., 2016 and 2017). The unique shape of the grooves in combination with the use of disc spring stacks allow for the desired self-centering behaviour. The angle of the grooves is designed in a way that at the time of unloading, the restoring force provided by the elastically compressed disc springs is greater than the opposing frictional resistance between the sliding plates. Consequently, the elastic force of the discs pushes back the slotted sliding plates to their starting position.

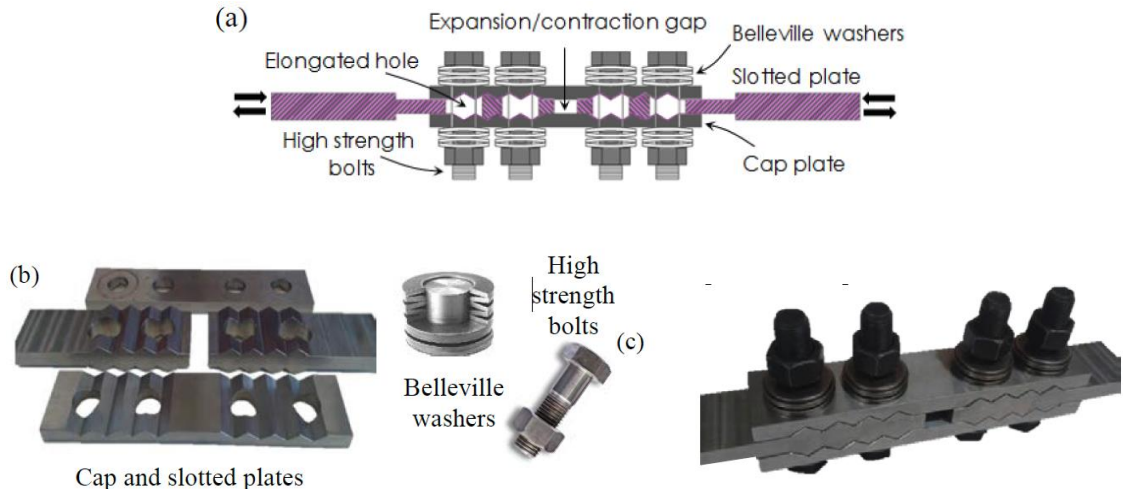

Fig 3-4. RSF joint: a) Section view, b) Components, c) Assemblage

It should be pointed out that the sliding plates can only travel the length of a single groove because their movement will be limited by the fully flattened (or locked) disc springs. The geometry of the grooves as well as the number of disc springs are calculated based on the force-displacement requirements for a targeted damping and ductility.

In addition, with the same clamping force through the use of high-strength bolts, the lateral resistance of this new joint could be higher than the common flat friction joints. Therefore, by applying this new friction joint, not only there is no requirement for adopting post-tensioning systems which would add to the cost of structure, but also the number of bolts could be decreased and subsequently the size of the joint and steel plates could be optimised.

An analytical design model has been developed to predict the RSFJ load resisting capacity based on the free-body diagrams depicted in Figures 2-5 and 2-6 (Zarnani et al., 2015). The slip force (F_{slip}) for a symmetrical arrangement can be estimated by Eq. (1). Note that this design method is for the symmetrical case. For more detail about the dissimilarities between the symmetric and asymmetric friction joints, please see (Zarnani et al., 2016).

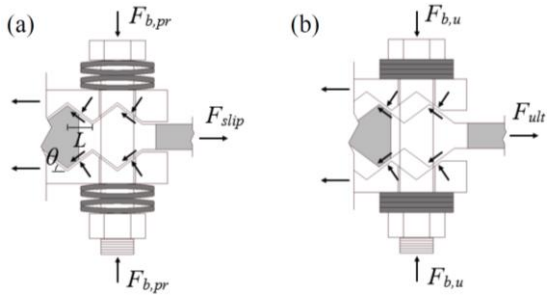

Fig 3-5. Free body diagram for loading of symmetric RSF joint: (a) friction plates at rest before slip, (b) friction plates at ultimate loading

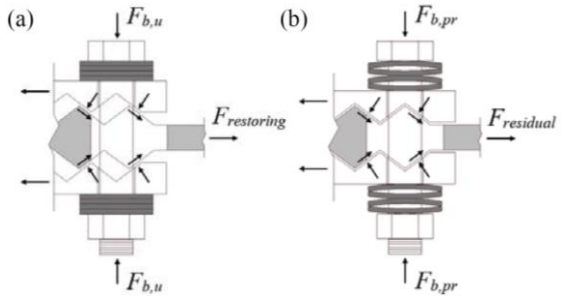

Fig 3-6. Free body diagram for unloading of symmetric RSF joint: (a) friction plates at ultimate unloading, (b) friction plates at restored position

The slip force (F_{slip}) for a symmetric configuration can be determined by Eq. (1)

$$F_{slip} = 2n_b F_{b,pr}\left(\frac{\sin\theta + \mu_s \cos\theta}{\cos\theta - \mu_s \sin\theta}\right) \quad (1)$$

Where $F_{b,pr}$ is the clamping force in the bolt due to pre-stressing of the Belleville washers, n_b is the number of bolts, θ is the angle of the grooves and μ_s is the static coefficient of friction. Figure 3-7 shows a schematic diagram of the hysteresis loop of the RSFJ. The residual resistance of the joint at the end of the unloading can be calculated by Eq. (2) Here, μk is the kinetic coefficient of friction which can be considered as 0.85 μs.

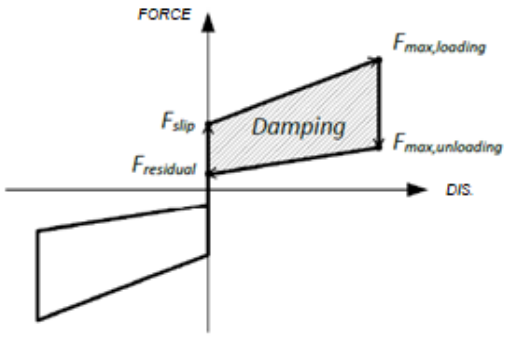

Fig 3-7. Schematic load-deformation loop for RSF joint

$$F_{residual} = 2n_b F_{b,pr}\left(\frac{sin\theta - \mu_k cos\theta}{\cos\theta + \mu_k sin\theta}\right) \quad (2)$$

The ultimate force at the loading ($F_{ult,loading}$) and unloading ($F_{ult,unloading}$) stages can be determined by changing μs and $F_{b,pr}$ in Eq. (1) and Eq. (2) with μ_k and $F_{b,u}$, respectively. The ultimate force in the bolt ($F_{b,u}$) can be calculated by Eq. (3) in which k_s and Δ_s are the total stiffness of the stack of washers and their maximum deflection when they become totally flattened.

$$F_{b,u} = F_{b,pr} + k_s \Delta_s \quad (3)$$

The maximum deflection in a RSFJ is determined by Eq. (4) where n_j is the number of joints that act in series (for example, n_j is equal to 1 for a single acting joint and 2 for a double acting joint).

$$\delta_{\max} = n_j \frac{\Delta_s}{\tan\theta} \tag{4}$$

The joint provides a restoring feature if Eqs. (5) and (6) are satisfied. In Eq. (6), L shows the horizontal distance between the top and the bottom of the groove.

$$\mu_s < \tan\theta \tag{5}$$

$$L > \frac{\Delta_s}{\sin\theta} \tag{6}$$

In this symmetrical arrangement, the bolts do not transfer shear forces and are only subject to tensile stress. The steel plates need to be designed to take the tensile and compressive forces at the time of cyclic loads. Additionally, the potential bending of the cap plates (to be designed as a beam under point loads) needs to be taken into account.

3.3. Connection Parameters effects

The cyclic hysteresis loops illustrated in Figures 2-8 to 13 demonstrate the impact of connection parameters on its performance. The effect of connections variations is studied in the value of slip force, ultimate capacity, restoring force, residual resistance, joint deformation, as well as the hysteresis damping ratio (ξ_{hyst}).

The connection parameters investigated comprise the groove angle, the coefficient of friction (COF), the number of series and parallel disc springs, the number of the bolts, and the initial pre-stressing force in the bolts.

The difference between the F_{ult} and $F_{restoring}$ magnitudes implies the frictional resistance that has to be overcome at the time of unloading to return the joint to its initial position. As appeared in Figures 3-8 and 13, by embracing a higher CoF (by changing the material arrangements of the sliding surface) and expanding the clamping force (through utilizing more bolts), the frictional resistance increases correspondingly, as theoretically anticipated.

By comparing the impact of connection parameters on the hysteresis damping ratio, it can be deduced that only increasing the angle of groove has an inverse effect on the ξ_{hyst}. Increasing the CoF, the number of discs in parallel, as well as the pre-stressing force result in a higher ξ_{hyst}, whereas adding to the number of discs in series and the number of bolts have no impact.

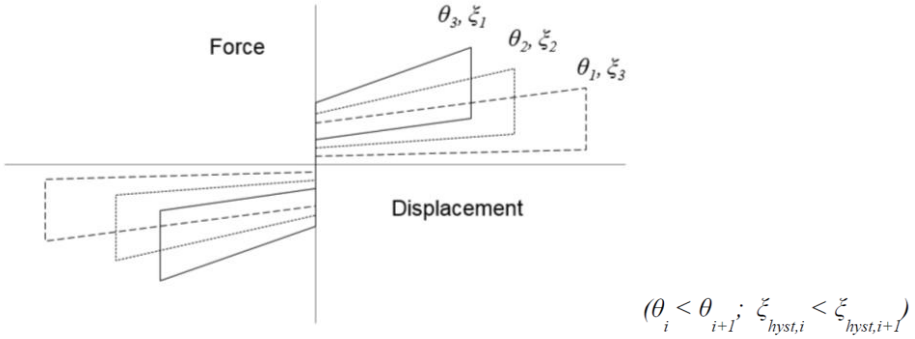

Fig 3-8. Groove angle effect (Zarnani et al., 2016)

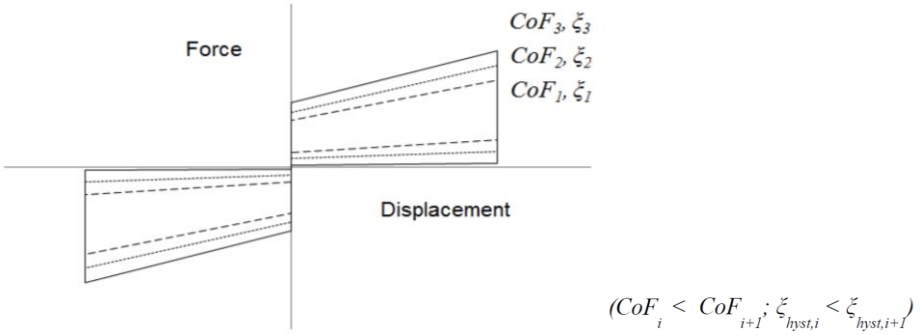

Fig 3-9. Coefficient of friction effect (Zarnani et al., 2016)

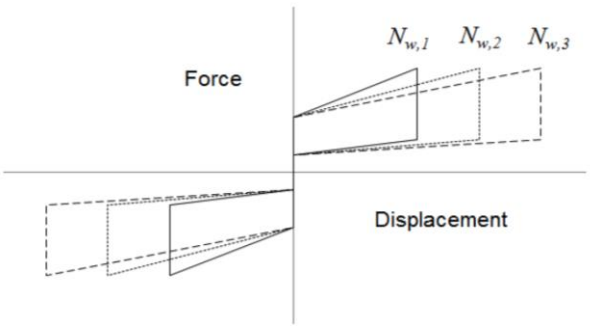

$(N_{w,i} < N_{w,i+1}; \xi_{hyst,i} = \xi_{hyst,i+1})$

Fig 3-10. Effect of number of washers- in series (Zarnani et al., 2016)

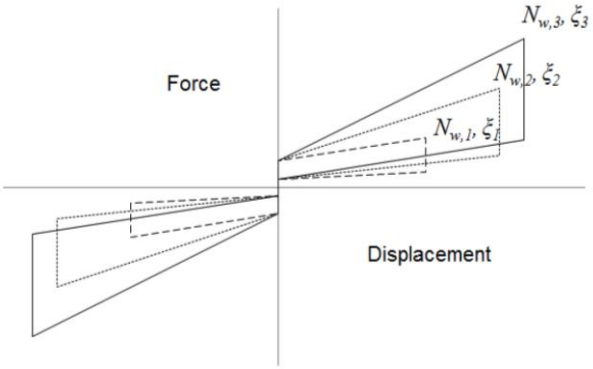

$(N_{w,i} < N_{w,i+1}; \xi_{hyst,i} > \xi_{hyst,i+1})$

Fig 3-11. Effect of number of washers- in parallel (Zarnani et al., 2016)

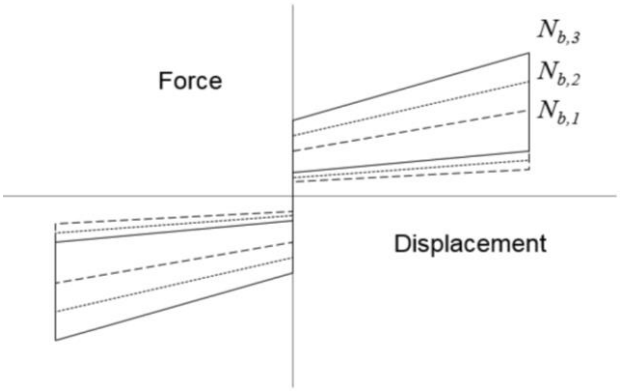

$(N_{b,i} < N_{b,i+1}; \xi_{hyst,i} = \xi_{hyst,i+1})$

Fig 3-12. Effect of number of bolts (Zarnani et al., 2016)

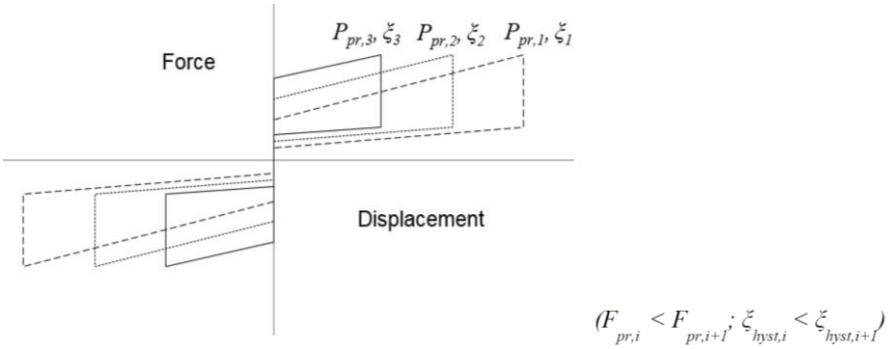

Fig 3-13. Effect of pre-stressing force (Zarnani et al., 2016)

3.4. RSFJ Anti-Locking Mechanism

The design of the RSFJ is intended to ensure that all the components within the RSFJ itself or the adjacent structure remain in the elastic region and the desired hysteriss behaviour is given bythe controlled sliding displacement within the RSFJ. To prevent the collapse in the cases where the applied loads exceed the design seismic loads, a secondary fuse is considered in the RSFJ. When the RSFJ comes to its most extreme capacity and the ridges are locked, the clamping bolts (or rods) begin to yield.

The plastic elongation of the bolts gives extra travel distance for the joint permitting it to preserve ductile behaviour up to and even more than the collapse limit state of the structure. This implies that when the RSFJ is designed for Ultimate Limit State (ULS) seismic loads (ordinarily corresponds to 2.5% of inter-story drift), ductile behaviour can be given upto the maximum Credible Earthquake (MCE), which is typically near to 4% of inter-story drift.

The specifications of the clamping bolts (or rods) determine the behavior of the RSFJ after the secondary fuse is activated. Figure 3-14(a) shows the specifications of the clamping bolts in which k_{fuse}, plastic is the effective plastic stiffness of the bolts after yielding up to the ultimate force ($F_{ult,fuse}$) before necking happens. In the RSFJ, as shown in Figure 3-15(b), the ridges are locked and the disc springs are flat at the maximum capacity of the joint ($F_{RSFJ,ult}$). At this stage,

the clamping bolts start to yield providing more deformation capacity for the joint. The yielding of the bolts decreases the design slip force in the RSFJ ($F_{RSFJ,slip}$) but the self-centering behaviour is not compromised.

The characteristics of the clamping bolts (or rods) determine the behaviour of the RSFJ after the secondary fuse is triggered. Figure3-14(a) depicts the characteristics of the clamping bolts in which $k_{fuse,plastic}$ is the effective plastic stiffness of the bolts after yielding up to the extreme force ($F_{ult,fuse}$) before necking stage. Within the RSFJ, as appeared in Figure 3-14(b), the ridges are locked and the disc springs are fully flat at the ultimate capacity of the joint ($F_{RSFJ,ult}$).

At this stage, the bolts begin to yield allowing for a greater deformation capacity in the joint. The yielding of the bolts reduces the slip force on the RSFJ ($F_{RSFJ,slip}$) in the subsequent cycles, however, the self-centering aspect till is not compromised.

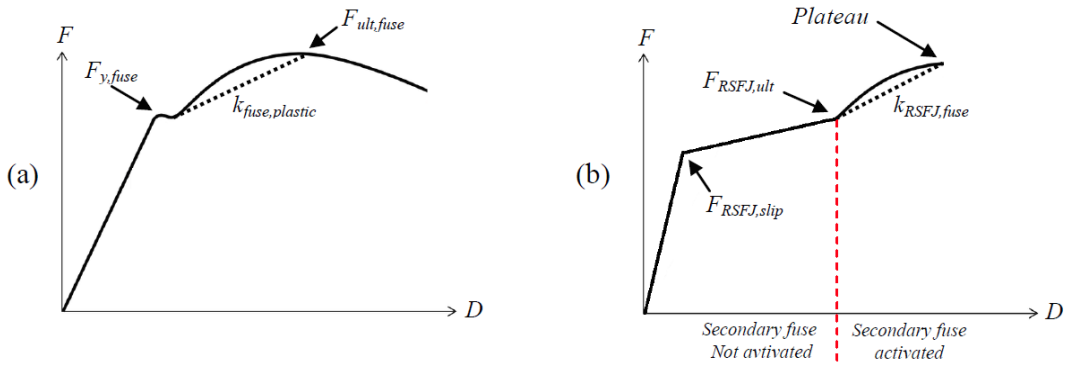

Fig 3-14. Behaviour of the RSFJ with the secondary fuse: a-load-deformation curve of clamping bolts (or rods) b-load-deformation curve of the RSFJ (Hashemi et al., 2018)

The effective stiffness of the RSFJ after the secondary fuse actuated ($k_{RSFJ,fuse}$) can be calculated by Eq. 7.

$$k_{RSFJ,fuse} = 2k_{fuse,plastic}\left(\frac{\sin^2\theta + \mu_s \sin\theta\cos\theta}{\cos^2\theta - \mu_s \sin\theta\cos\theta}\right)n_{rod} \quad (7)$$

Where n_{rod} is the number of bolts (or rods) in the RSFJ. A joint component test was conducted to experimentally verify the behaviour of the RSFJ and the secondary fuse (Hashemi et al., 2018). Figure 3-15 shows the test setup.

The RSFJ specimen had two cap plates and two slotted middle plates all made with high strength steel (F_y=700 MPa). For this test, fully threaded M18 rods (grade 8.8) were used to clamp the sliding plates.

The RSFJ specimen were previously designed for three rows and two columns of clamping bolts on each side (12 in total). However, because of the force limit in the MTS actuator (950 kN), only four rods per side were used for this test. Three-disc springs with 1.75 mm deformation capacity and 132 kN load capacity were used per rod per side. Two high strength nuts were used on both sides of the rods to avoid yielding in the threads before the rod itself.

Fig 3-15. Experimental testing of the RSFJ with the secondary fuse

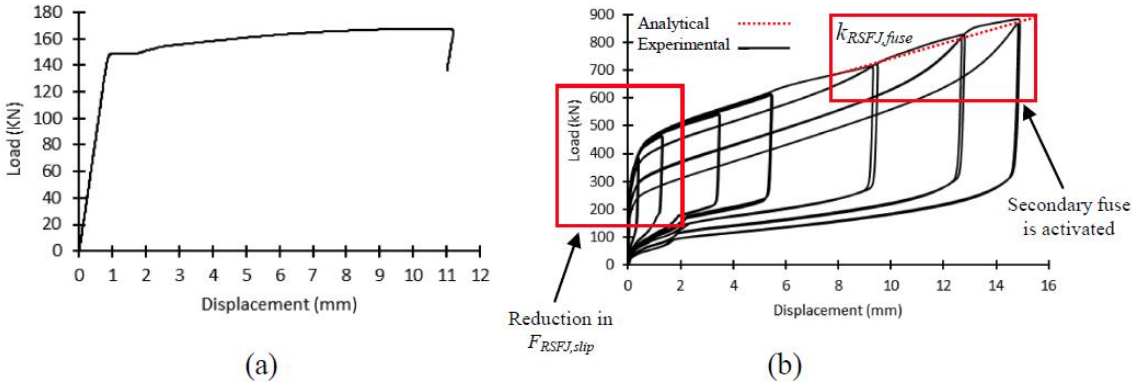

Fig 3-16. Experimental results of the RSFJ with the secondary fuse: a-load-deformation curve of the M18 rod grade 8.8 b-load-deformation curves of the RSFJ (Hashemi et al., 2018)

Prior to the RSFJ tests, a series of component tests were performed on the rod samples to investigate their performance characteristics. Figure 3-16 (a) shows the load-deformation curve of one of the rods as a typical sample. As can be seen, the rod has $F_{fuse,y}$=145 kN and $F_{fuse,ult}$ = 165 kN, k_{fuse}=1835 n/mm and 5% elongation considering its initial length. From Eq. 7, it is found $k_{RSFJ,fuse}$ =19671 N/mm. Fig. 3-16 (b) shows the results of the cyclic test on the RSFJ prior and after activating of the secondary fuse. The joint was designed to get locked at 8mm deformation. The top red rectangle in Figure 3-16 (b) illustrates the area where the rods started to yield. It can be found that the analytically calculated stiffness of the RSFJ after locking is in agreement with the test observation. In addition, it is noticeable that the slip force gradually alleviates after the secondary fuse is triggered.

4. Damage avoidance moment resisting frames (MRFs) using RSFJ

4.1. Purely pinned connection with RSFJ

The general concept of damage avoidance steel MRFs with RSFJs is demonstrated in Figure 4-1. In this new system, the RSFJ is located along the beam bottom flange and consists of two middle plates and two cap plates. The two middle plates (with elongated holes) are attached to the beam bottom flange and the column from each end. The two cap plates are clamped to the middle plates, and friction is generated when the middle plates slide against the cap plates. A pin is used at the top that can transfer the shear forces as well as the axial loads. Since pure pin has almost a zero-construction tolerance, a shim plate may be used between the pin bracket end plate and the column flange.

It should be noted that the connection detail shown in Figure 4-1 is one of the possible options. A more conventional assembly could be the one developed for the SHJ in which the pin action is provided by the elastic bending deformation of a plate connected to the beam top flange as well as another plate connected to the web transferring the shear force (Clifton et al., 2005). Nevertheless, the overall connection behaviour could be assumed similar given the top plate in the SHJ provides the required hinge action.

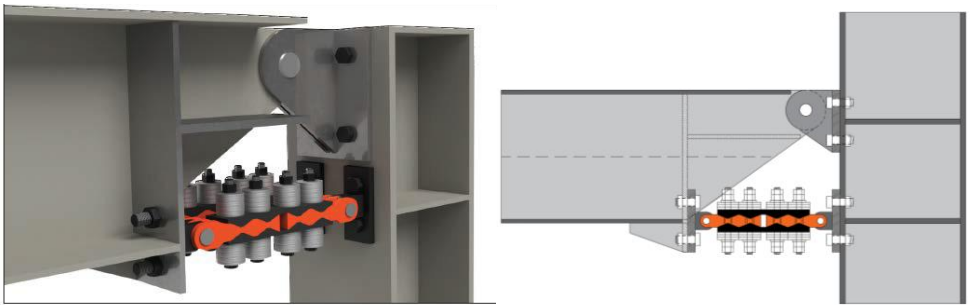

Fig 4-1. The concept of self-centring MRF with RSFJ - general arrangement

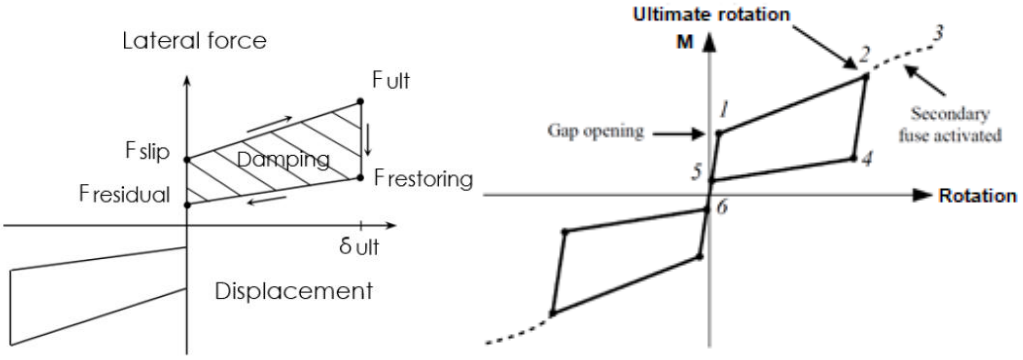

Fig 4-2. The concept of self-centring MRF with RSFJ: (a) hysteresis response of RSF joint (b) theoretical moment connection hysteresis loop

4.2. Connection analytical modelling

The relationship between the moment in the beam at the column face (M) and the relative rotation between the beam and the column (θr) is described in this section through a step design. Under the applied loading, the connection has an initial stiffness similar to that of a fully restrained bolted moment connection, where θr is negligible. In this phase, the elastic stiffness of the RSFJ governs the stiffness of the connection. The stiffness of the entire system mostly depends on the beam and column stiffnesses given the connection could be assumed to be relatively fixed.

Once the applied moment overcomes the frictional resistance in the RSFJ, the rotation and gap opening are imminent (stage 1 in Fig. 4-2). Eqs. 3 and 4 determine the moment capacity of the connection at the slipping point.

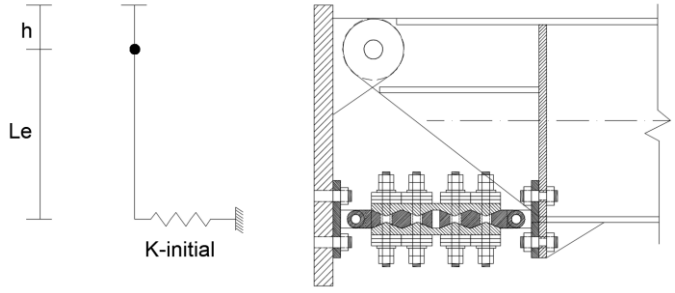

Fig 4-3. Analytical model of connection before slip

$$M_{slip}=F_{slip} . L_e = (K_{initial} . L_e . \Theta_{slip}) . L_e = (K_{initial} . L_e^2) . \Theta_{slip} = K_{\Theta,initial} . \Theta_{slip} \quad (3)$$

$$K_{\Theta,initial} = K_{initial} . L_e^2 \quad (4)$$

Where M_{slip} and Θ_{slip} are the moment and rotation at the connection corresponding to the RSFJ slip force (F_{slip}). L_e is the eccentricity of the RSFJ with respect to the pin position. $K_{\Theta,initial}$ and $K_{initial}$ are the connection rotational and RSFJ axial initial stiffnesses, respectively. After sliding, the moment capacity of the connection increases because of the compaction of the disc springs creating additional axial resistance in the RSFJ. The connection will be at its maximum moment capacity, M_{ult} (stage 2) when the RSFJ reaches the ultimate capacity $F_{RSFJ,ult}$. Eqs. 5 and 6 show the ultimate moment capacity of the connection at the joint ultimate deflection.

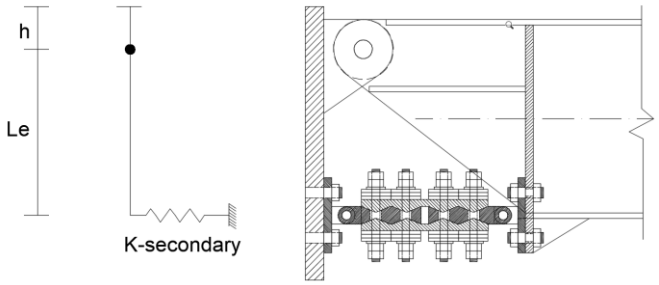

Fig 4-4. Analytical model of connection after slip

$$M_{ult}=M_{slip} + M_{ult-slip} \quad (5)$$

$$M_{ult-slip}=F_{ult-slip} . L_e = (K_{secondary} . L_e . \Theta_{ult-slip}) . L_e = (K_{secondary} . L_e^2) . \Theta_{ult-slip}$$

$$M_{ult-slip} = K_{\Theta-secondary} . \Theta_{ult-slip} \quad (6)$$

Where $K_{secondary}$ is the axial stiffness of the joint after slip and $M_{ult-slip}$ is the portion of the connection moment capacity added after the slip, corresponding to the force increase in the RSFJ from the slip point up to the ultimate point ($F_{ult-slip}$). It should be noted that if the load in the RSFJ continues to increase to more than $F_{RSFJ,ult}$, the secondary fuse can be activated (from

stage 2 to stage 3). When the RSFJ reaches its maximum capacity and the ridges are locked, the clamping bolts (or rods) start to yield. The plastic elongation of the rods provides additional travel distance for the joint allowing it to maintain a ductile behaviour up to and even more than the collapse limit state of the structure. This means that when the RSFJ is designed for Ultimate Limit State (ULS) seismic loads (corresponding to about 2.5% of inter-story drift), a ductile behaviour can be provided up to the Maximum Credible Earthquake (MCE), which could be close to 4% of inter-story drift.

Upon unloading (from stage 2 to stage 4), the variation in θr is insignificant given it is the elastic rotation which is reversed. Between stages 2 and 4, the moment contribution from the RSFJ changes its direction due to the reversal friction force. Between stages 4 and 5, θ_r reduces significantly as the beam comes back in contact with the column flange and the RSFJ gets fully closed. Between stages 5 and 6, the moment drops to zero as the residual force in the RSFJ decreases and accordingly there will be no rotation in the connection. A similar moment-rotation behaviour is expected during the positive moment (opposite direction) in which the RSFJ is loaded under compression.

It should be noted that in case of having a concrete slab on top of the steel beam, the stiffness of the slab can affect the behaviour of the connection. However, the effect of the slab is not investigated in this research project and will be further studied in the future.

4.3 Structural numerical modelling

This section briefly describes the numerical modelling and analysis of conceptual steel MRFs equipped with RSFJs. The flag-shaped hysteresis of the RSFJ can be modelled using conventional packages such as ABAQUS, SAP2000 and ETABS though properly calibrating the design parameters. To study the behaviour of the RSFJs, a prototype joint is modelled. Input data shows the specifications of the joint including the geometric properties, friction

coefficient and specification of the disc springs. The numerical results of the proposed model showed to be in good agreement with the analytical predictions. In the next chapter, it will be found that the experimental flag shaped behaviours are in line with the model predictions.

4.3.1 Finite Element Modelling in ABAQUS

For the FE modelling of the RSFJ in ABAQUS (Hibbitt et al. 2014), the following steps have been followed:

Step 1. Input data: The input parameters used for the modelling were based on the component test performed by Hashemi et al. (2017), as shown in Table 4-1. Figure 4-5 depicts the assembly of the manufactured specimen comprised of two middle slotted plates and two cap plates.

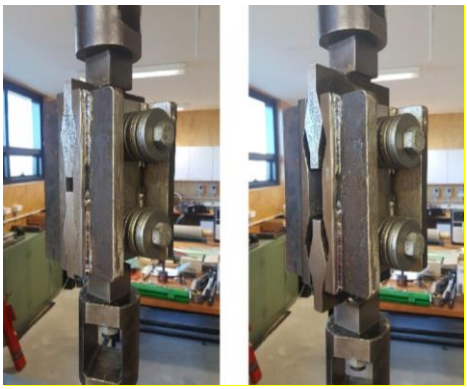

Fig 4-5: Component test: before slip (Left) and after slip (Right) (Hashemi et al. 2017)

Table 4-1 presents the design parameters of the manufactured RSF joint. The slip force (Fslip) for the test was set as 24 kN.

Table 4-1: Characteristics of the tested RSFJ

Parameter	**Value**	**Design Parameter**	**Value**
Angle of the grooves	35	Disc spring thickness (mm)	6.5
Number of bolts (n_b)	1	Disc spring overall height (mm)	8
μ_s	0.19	Disc spring internal height (mm)	1.5
Slotted whole length (mm)	35	Disc spring outside diameter (mm)	70
Each washer capacity (kN)	110	Disc spring inside diameter (mm)	21
n_s (Per bolt)	9		

Step 2. Modelling: in this step half of the joint assembly has been modelled to optimize the analysis time.

Step 3. Define the bolts, discs and prestressing force: the spring link option of the software can be used for modelling of the bolts and discs stiffnesses (Figure 4-6(a)). The prestressing force can be defined as an area load (Figure 4-7(b)).

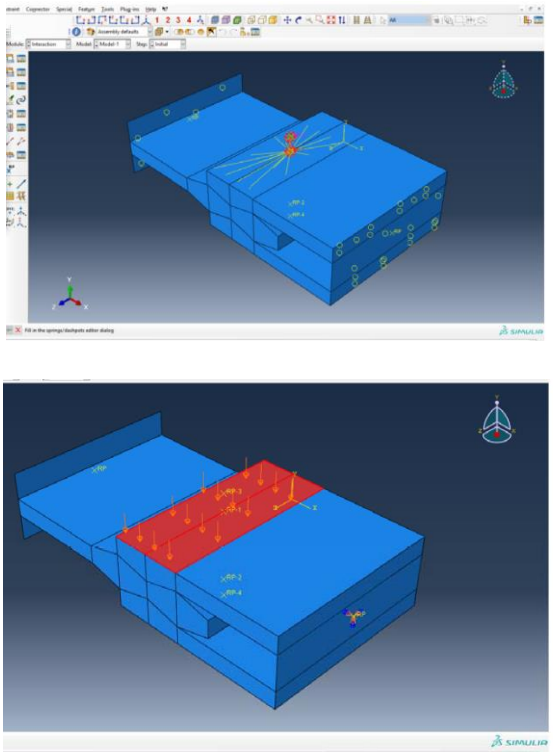

Fig 4-6. Modelling of RSFJ in ABAQUS: a) defining bolts, b) defining pre-stressing

Step 4. Define the cyclic displacement: two cycles of displacement equal to 30mm and 60mm have been defined in ABAQUS.

$$D = V \times t\ (time\ step = 0.1s) \rightarrow \quad D_1 = 1 \times 0.3 \times 0.1 = 0.03\ m\ ,\ D_2 = 1 \times 0.6 \times 0.1 = 0.06\ m \qquad (7)$$

Step 5. Define the contact friction: the friction has been defined as a tangential force. In the Interaction module of the software, “All with self” has been selected so that the friction is considered between all the surfaces in contact.

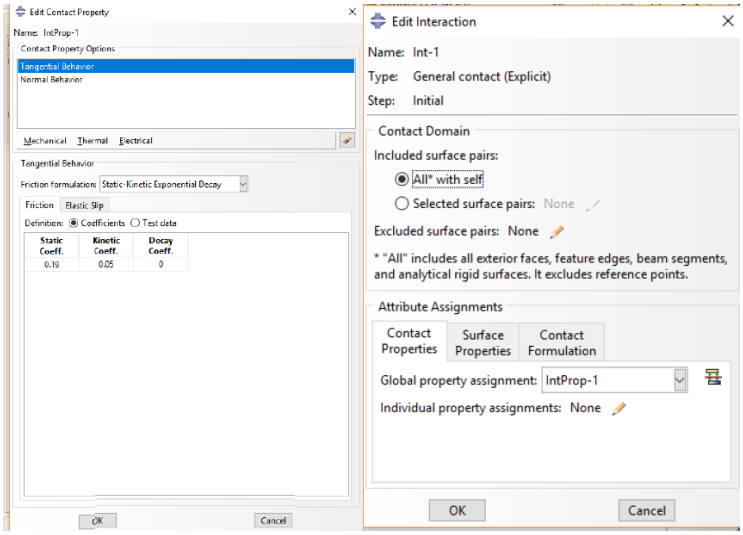

Fig 4-7. Defining friction between the plates in the RSFJ model in ABAQUS

Step 6. In this step, the model has been meshed (Figure 4-8)

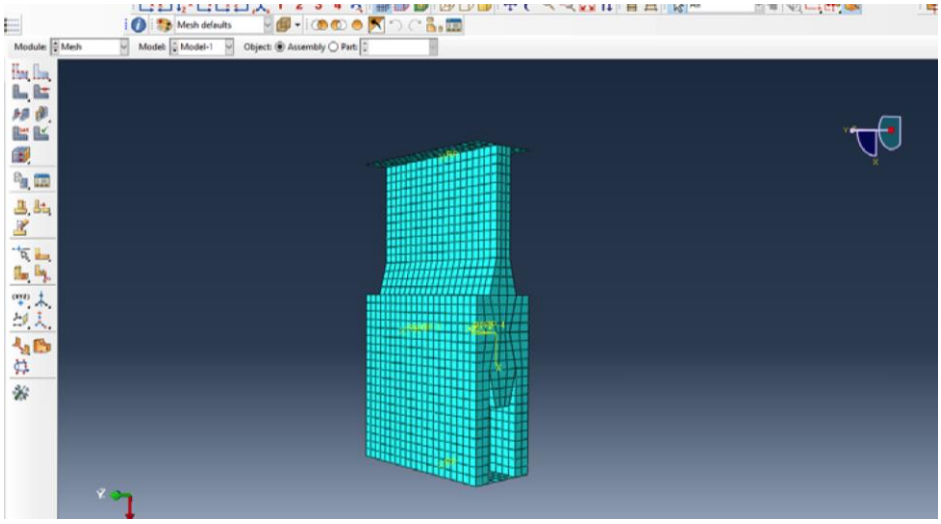

Fig 4-8. Meshing of friction plates in the RSFJ ABAQUS model

Step 7. The steps of the analysis are defined.

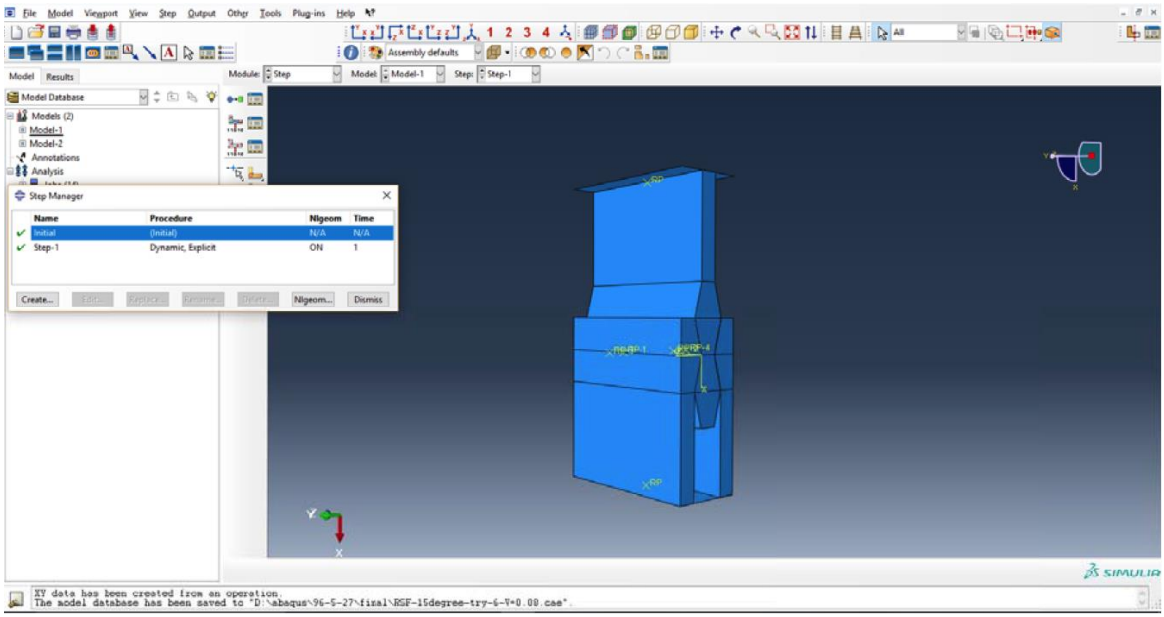

Fig 4-9. Defining the steps of the analysis

Step 8. As the final step, the analysis has been run and the results have been compared with the analytical predictions using the method explained in section 3.2 (Figure 4-10).

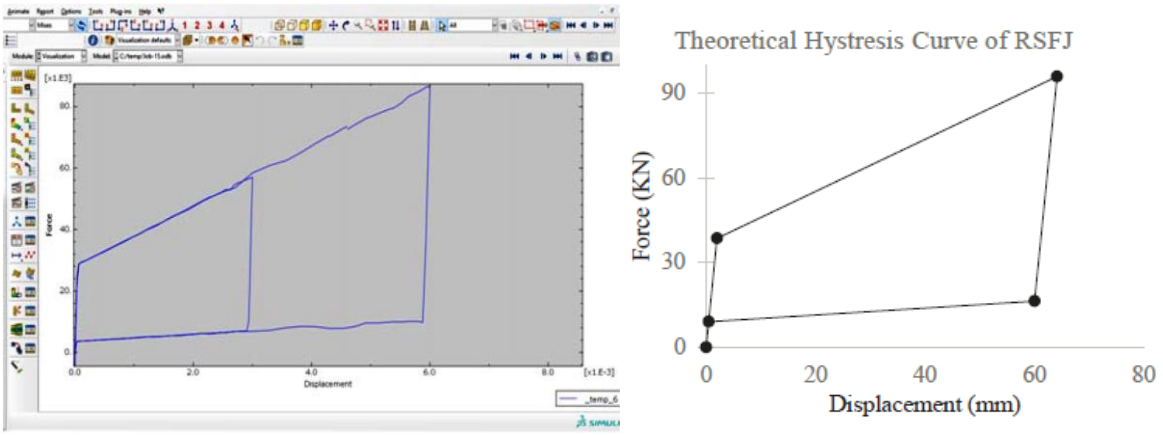

Fig 4-10. Comparison of numerical results with analytical predictions

4.3.2 Modelling in SAP2000

The RSFJ can be also integrated in the structural analysis and design programs such as ETABS and SAP2000 (CSI, 2011). It allows the designer to accurately calibrate the parameters according to the requirements of the project. In ETABS/SAP2000, the RSFJ can be modelled using the "Damper – Friction Spring" link Element.

This function accurately represents the flag-shaped hysteresis of a RSFJ by properly calibrating the input values in accordance with the design parameters of the joint. The parameters can be defined for any of the six translational or rotational degrees of freedom.

The design parameters of the RSFJ are: F_{slip} (slip force of the RSFJ), F_{ult} (ultimate force in the RSFJ at the end of loading), $F_{restoring}$ (restoring force of the RSFJ), $F_{residual}$(residual force in the RSFJ at end of unloading), Δ_{slip} (initial elastic deflection of the RSFJ before slip), Δ_{ult} (ultimate displacement of the RSFJ), $K_{initial}$ (initial stiffness of the RSFJ before slip), $K_{loading}$ (loading stiffness of the RSFJ) and $K_{unloading}$ (unloading stiffness of the RSFJ).

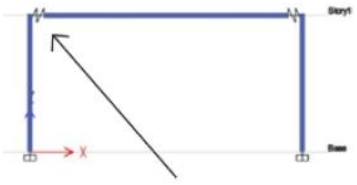

Rotational link element representing the beam-column behavior of the MRF connection with the RSFJ

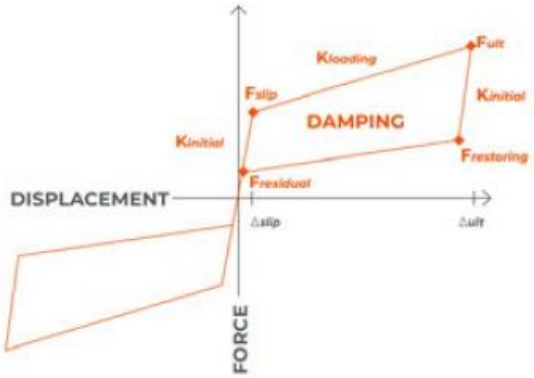

Fig 4-11. RSFJ Modelling in Sap2000 (top), Design input parameters (bottom)

The recommended approach to model the MRFs with RSFJs is to model the moment-rotation behaviour of the beam-column connection using a single link element. The link element can be attached to the beam and column at their contact interface. The moment-rotation behaviour of the MRF connection can be specified corresponding to the force in the RSFJ (F_{RSFJ}) and the lever arm (Le) which is the vertical distance between the centre of the RSFJ and the rotating pivot close to the top beam flange. For this case, the parameters should be defined for the relevant rotational degree of freedom (for example, R3 in case of the global "XZ" plane). The other five degrees of freedom should be "fixed". The active direction should be defined as "Both" given the link element works in both directions.

The Damper – Friction spring design parameters are determined, as follows:

- Initial (Non-slipping) Stiffness = $K_{\theta,initial} = K_{initial} \times L_e^2$
- Slipping Stiffness (Loading) = $K_{\theta,loading} = K_{secondary} \times L_e^2$
- Slipping Stiffness (Unloading) = $K_{\theta,unloading} = K_{unloading} \times L_e^2$
- Pre-compression displacement = $(-M_{slip}) / K_{\theta,loading} = - [K_{initial} \times L_e^2) \times \Theta_{slip}] / [K_{secondary} \times L_e^2] =$
  $= - (K_{initial} / K_{secondary}) \times \Theta_{slip}$
- Stop displacement = Θ_{ult}

By defining these parameters, the rest of the RSFJ parameters (Θ_{slip}, M_{ult}, $M_{restoring}$ *and* $M_{residual}$) will be automatically calculated. To study the behaviour of the steel MRFs with RSFJs, a prototype frame is considered. Figure 4-12 shows the specifications of the frame including the geometric properties and the frame sections. The frame is 4m wide and 3m high and the columns are pinned to the foundation. The beam and columns section were 250UB31.

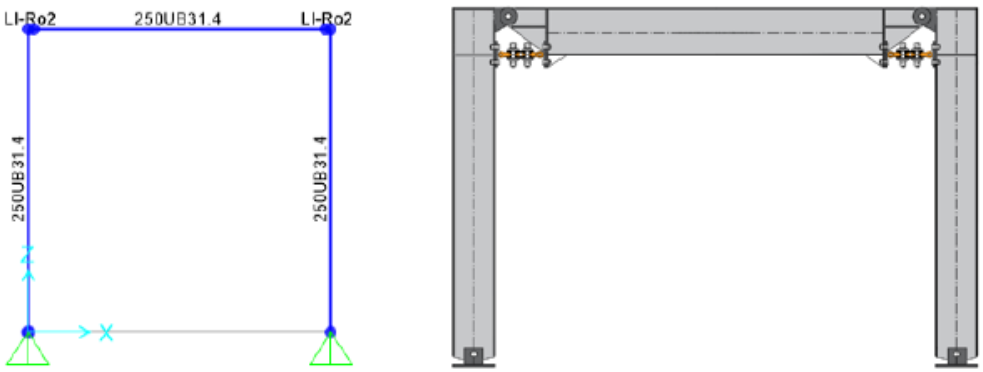

Fig 4-12. Sample MRF frame modelled with RSFJs in Sap2000

The required ULS moment capacity of the connections was assumed as 50 kN.m. The slip threshold for the RSFJs is specified as 50% of the ULS moment capacity. Table 4-2 shows the input data and the calculated design parameters for the MRF connections.

Table 4-2- Summary of the input data and design parameters for RSFJ

Input Parameter	**Value**	**Design Parameter**	**Value**
Angle of the grooves	35	Initial Stiffness (kN/mm)	7.6e6
n_b	1	Slipping Stiffness (Loading)	1.1e6
μ_s	0.19	Slipping Stiffness (Unloading)	0.55e6
$F_{b,pr}$ (kN)= 50% $F_{b,ult}$	61	Pre-compression displacement	2.2%
Each washer capacity (kN)	135	Stop displacement (Rad)	2.5%
n_s (Per bolt, each side)	2		

Push-over simulations were carried out for the frame equipped with the RSFJs in all the beam-column connections. The RSFJ load-slip curve as well as the moment-rotation hysteresis behaviour of the connections are shown in Figures 4-13(a) and (b). Figure 4-13 (c) shows the base shear and the maximum story drift. It can be found that the MRF connection shows a flag-shaped hysteresis with a fully re-centring behaviour.

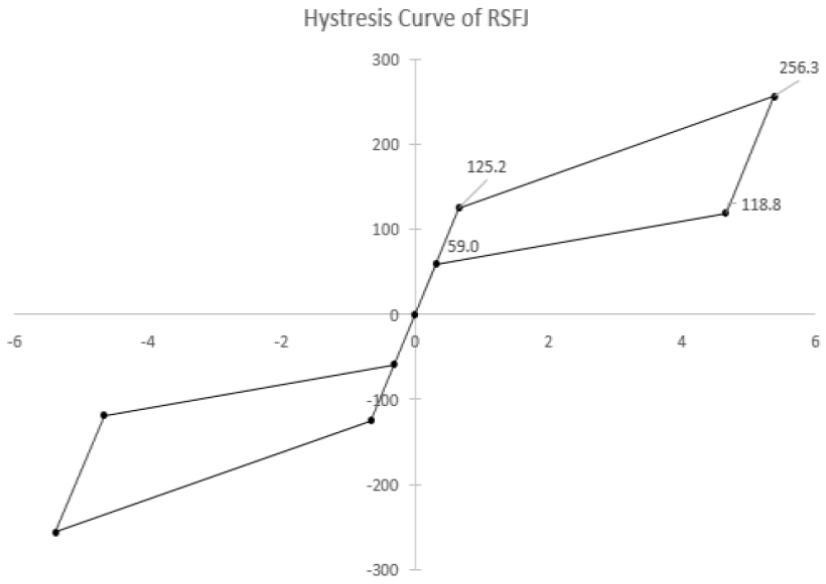

(a)

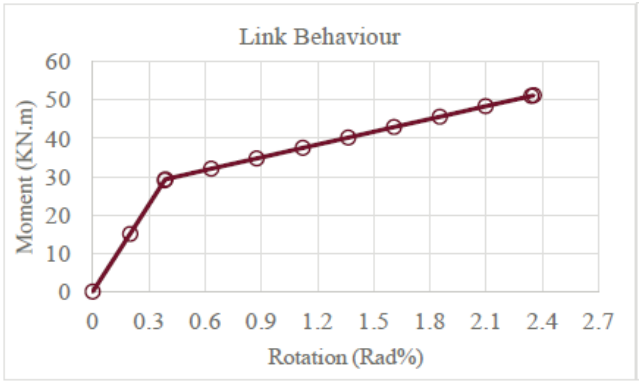

(b)

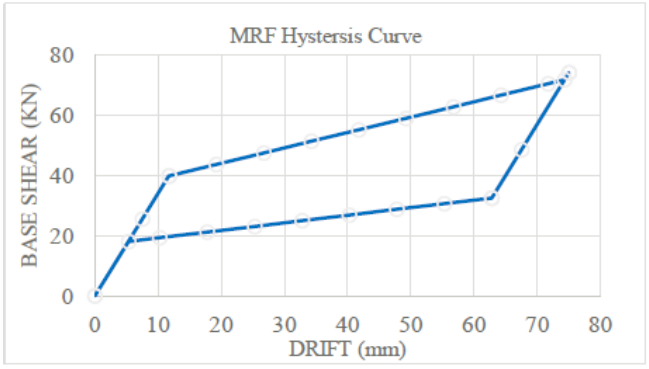

(c)

Fig 4-13. MRF modelled with RSFJs: a) RSFJ hysteresis behaviour, b) Connection behaviour, c) MRF hysteresis behaviour

4.4 Modelling of a conceptual 10-storey MRF building with RSFJs

In this section, a prototype 10-storey MRF building has been modelled in SAP2000 using RSFJs to investigate the seismic performance. The structure has been assumed to be an office building located in Auckland and was designed based on NZS3404. It had 3 bays at 8m in each direction, spanning 24m by 24m. The height of each storey was considered 3m resulting in overall building height of 30m. The building was a steel frame structure with composite floors. Figure 4-14 shows the 3D geometric model of the structure. The section sizes of the columns, fixed beams and pinned beams were SHS400/20, 530UB92 and 310UB40, respectively.

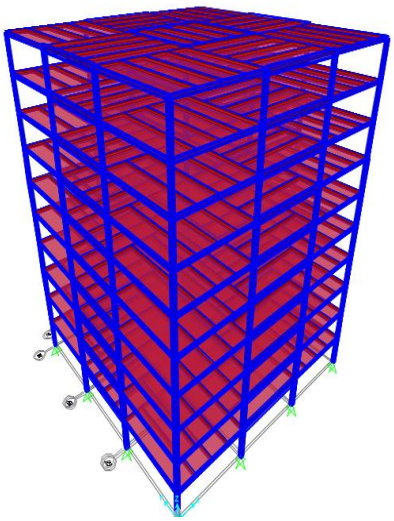

Fig 4-14. 3D model of the MRF structure with RSFJs

Table 4-3 presents the design parameters of the RSF joint used in the model.

Table 4-3: Characteristics of the tested RSFJ

Parameter	**Value**
Angle of the grooves	38
Number of bolts (n_b)	4
μ_s	0.19
$F_{b,pr}$ (KN)	61
Each washer capacity (kN)	135
n_s (Per bolt, each side)	5

In the first attempt, all the main and secondary beams have been modelled as simply supported except the 8 main steel beams which have been highlighted by the red bold lines in Figure 4-15 (Top) for which the RSFJs were adopted to provide moment connections. The static non-linear push over analysis was performed to find the behaviour of the structure based on this initial beam-column connection arrangement (Figure 4-15 (Bott.)).

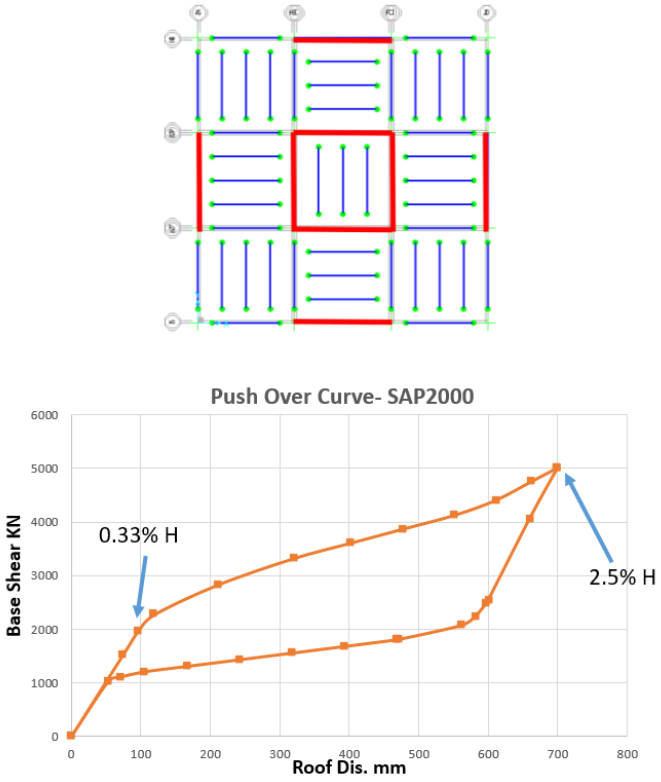

Fig 4-15. Position of moment frames with RSFJ joints in plans (Top), Push over analysis result (Bott.)

In the second attempt, all the beams only on the first floor were modelled with the RSFJ moment connections.

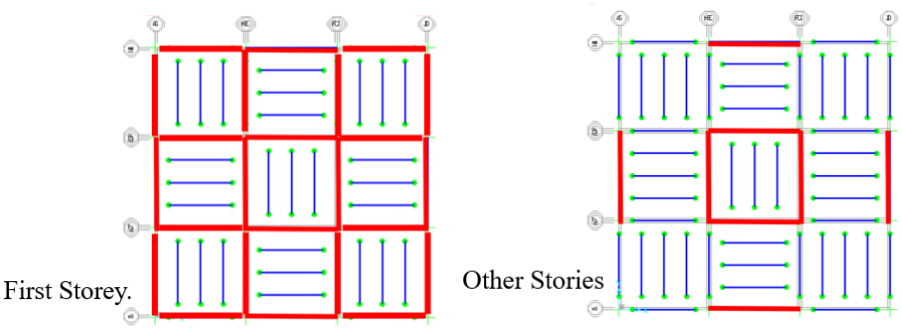

Fig 4-16. Position of moment frames with RSFJ joints in plans

As expected, in this model, the initial stiffness of the building increased as a result of adding more moment frames at the first floor. Also, the push over curve of the structure shows considerable increasing in the ultimate capacity and damping of the structure (Figure 4-17).

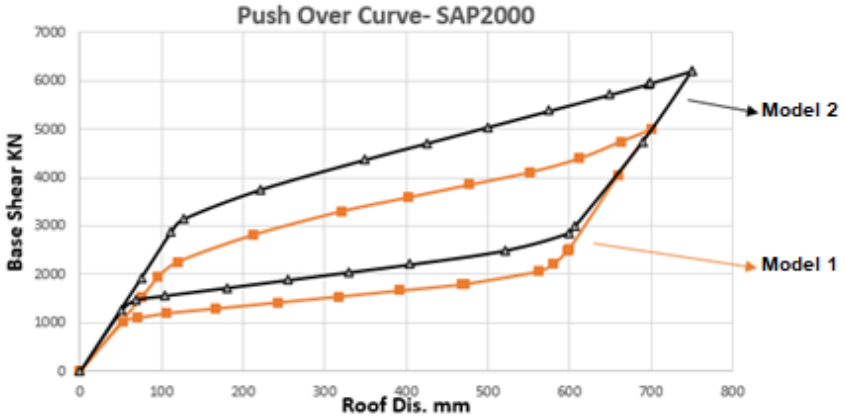

Fig 4-17. Comparing the push over response curves of the two models

The numerical results of the 10-storey MRF model with RSFJs shows a perfect flag shape behaviour of the structure. Using the RSFJs in connections has several advantages which have been listed, as follows:

1- Concentrating all the nonlinearity in the RSF joints. Therefore, all the members of the structure remain elastic during the earthquake and there would be no need for the structural repair after the event.

2- Achieving damage avoidant connections.

3- Decreasing the seismic demand given the damping and ductility provided for the structure.

4- No need for the use of RSFJ in all the connections of the structure. The number and location of the moment connections with RSFJs can be optimized.

5- All the pinned main and secondary steel beams can be designed as composite sections with concrete floor. This could decrease the size of the beams and the total structural cost.

5. Component testing of RSFJ

In order to experimentally investigate the hysteretic behaviour of the RSF joint, a set of symmetric RSF joints with the grooves angle of 25 degrees were designed, fabricated and tested under quasi-static loading. In this chapter, each step will be explained. The joints later have been adopted in the beam connection large scale testing.

5.1. Joint design

In this section, designing of the RSFJs has been explained. As the first step, the design parameters of the RSF joint were needed to be defined to achieve the target ultimate axial capacity and deformation. Since the joints were supposed to be fitted in a cantilever steel beam for the main large-scale testing, they had to be designed in consistent with the main beam geometry and its moment capacity. Designing of the beam setup will be explained in the next Chapter 5. According to the beam geometry and moment capacity, two RSF joints were required with the ultimate axial capacity of 220 kN at 12.5 mm ULS deflection. Summary of the joint parameters as well as the joint hysteresis behaviour (predicted using the analytical equations described in Chapter 3, are presented in Table 5-1.

Table 5-1- RSF joint parameters

Double-acting joint (two splices) with grease:		
Bolts and Plates		
n_b =	2.0	on each splice
$F_{b,pr}$ =	70.0	*kN*
$F_{b,ult}$ =	120.0	*kN*
θ =	24.0	°
$\mu_{s,g}$=	0.10	*with grease*

$\mu_{k,g}$=	0.085	($0.85*\mu s,g$)
$tan\ \theta$ =	0.44	($tan\ \theta > \mu s,g$)
Disc spring		
Disc thickness =	8.5	*mm*
Disc internal height =	1.35	*mm*
Disc capacity =	130	*kN*
RSFJ, pins and brackets initial deflection at F_{slip}=	3.7	*mm*
Number of discs per bolt, each side =	5.0	
Accumulated height of discs, each side (after pre-stressing) =	45.3	*mm*
Connection Performance		
Ratio of F_{slip}/F_{ult} =	3/4	
Total slip distance =	12.6	*mm*
Each splice slip distance =	6.3	*mm*
Disc deformation after pre-stressing =	2.8	*mm*
Disc internal height (after pre-stressing) =	0.56	*mm*
Hysteresis damping =	7.2%	*kN.m*
Initial stiffness =	43	*kN/m*
F_{slip} =	159.7	*kN*
$F_{ult, loading}$ =	219.4	*kN*
$F_{ult,unloading}$ =	158.5	*kN*
$F_{residual}$ =	121.3	*kN*

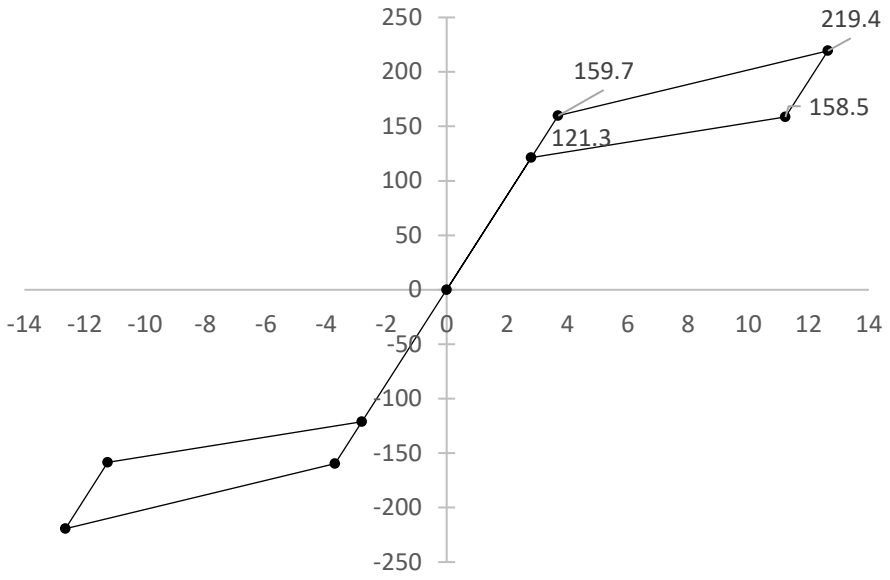

Fig 5-1. Predicted hysteresis curve of RSF joints

In the next step, all the components of the joint needed to be designed to take the axial load of 220 kN and remain fully elastic with no plastic deformation. For designing the components, an overstrength factor of 1.5 has been considered. The cap plates and slotted middle plates were made of mild steel grade 300, lubricated by a special grease to control the wearing and achieve a more uniform frictional behaviour between the sliding surfaces. Four high strength bolts with minimum tensile strength of 830 MPa (Grade 8.8) were employed (two bolts in each splice). The disc stacks on each side of each bolt were comprised of five discs in series with the flat load of 130 kN. The pre-stressing force on each bolt ($F_{b,pr}$) was 80 kN. The disc stacks were placed under the bolt nuts and the nuts were tightened until the desired pre-stressing force (80 kN) per bolt was achieved.

5.2. Joint manufacturing and assembly

After designing of the plates, the shop drawings were provided for the manufacturing. In Figures 5-2 and 5-3, the geometry of the joint plates is presented.

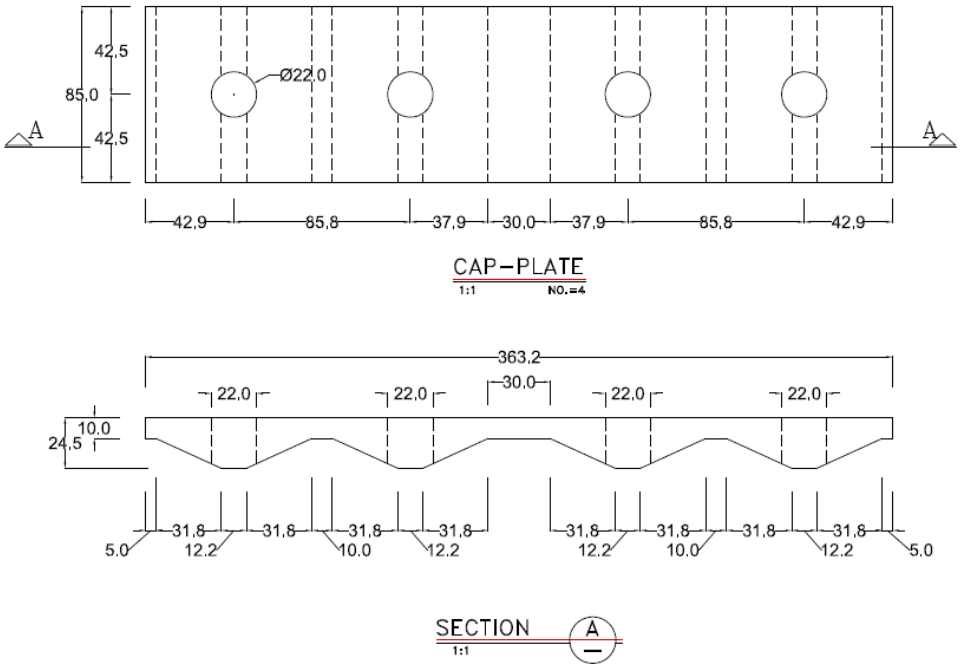

Fig 5-2. Cap plates shop drawings of the RSF joints

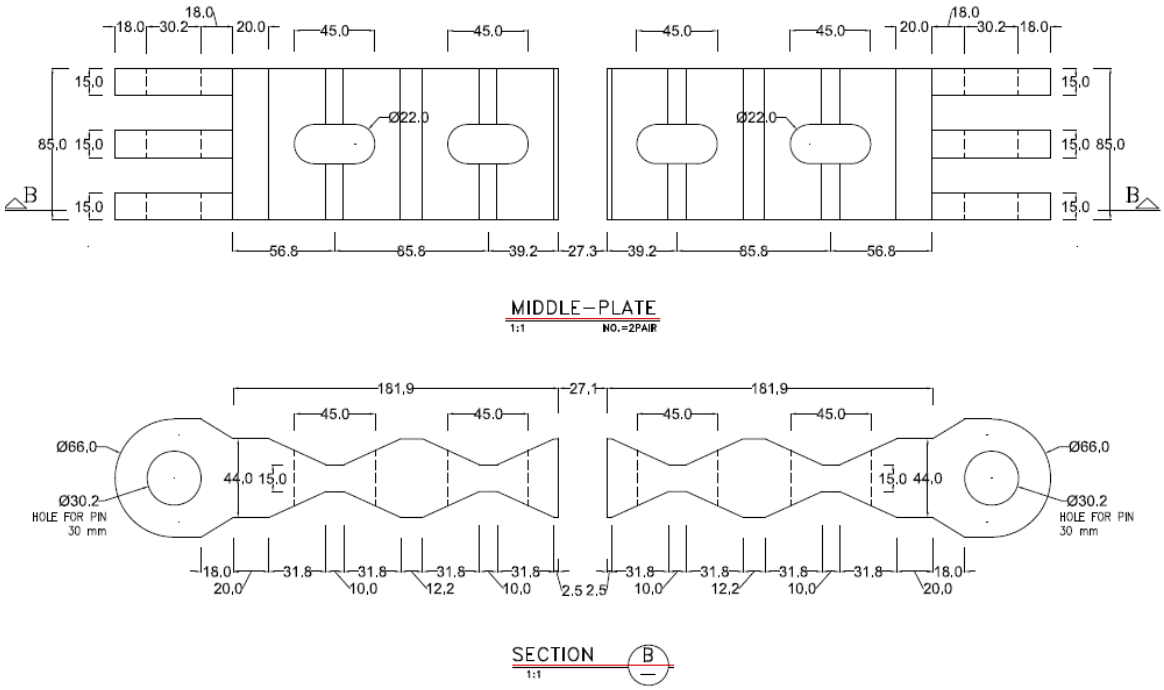

Fig 5-3. Slotted middle plates shop drawings of the RSF joints

The shop drawings have been sent to AUT's workshop for manufacturing. In Figure 5-4, the manufactured cap and middle plates of the joints have been shown.

Fig 5-4. Manufactured joints

After manufacturing of the joints, they were painted and got prepared for assembly and pre-stressing. As explained in the previous section, the rods and discs had to be pre-stressed at 80 kN. To control any possible adjustments in the discs stack affecting the prestressing force, they were fully compacted three times before the final pre-stressing. In Figure 5-5, the assembled RSF joint has been shown at the stage which the disc stacks were fully compacted under 130 kN.

Fig 5-5. Assembled RSF joint with fully compacted discs

After full compaction of discs, they were pre-stressed at 80 kN using the prestressing tool at AUT's Structures lab including. The prestressing tool was comprising a jack and load cell allowing to precisely monitor the level of load being applied. Due to health and safety measurements, the prestressing process was done under the supervision of lab technicians.

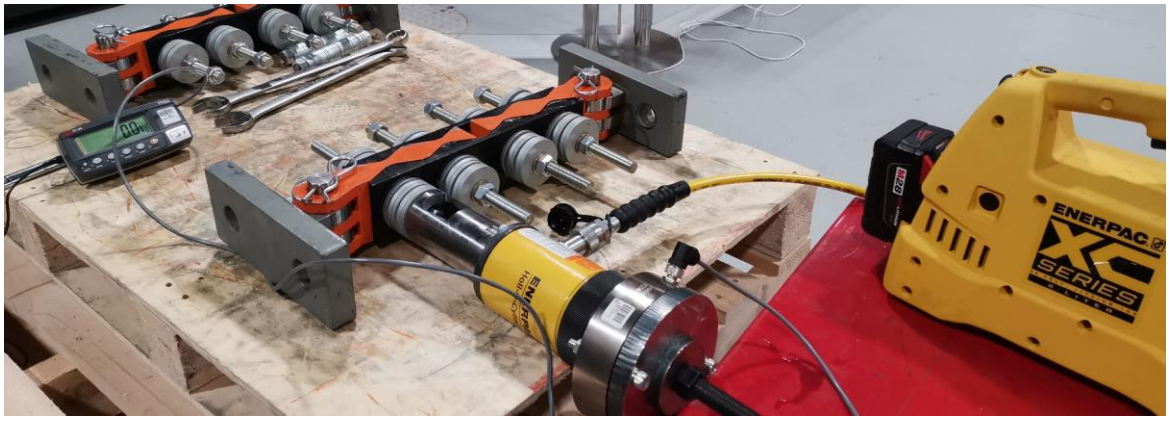

Fig 5-6. Pre-stressing of the RSF joints using the jack and load cell

5.3. Test results and discussion

In order to experimentally investigate the hysteretic behaviour of the RSF joint, a test under quasi-static loading was conducted using a Universal Testing Machine (UTM). The UTM system is comprised of a load frame, electronic frame controller, and testing software. The load frame has a rectangular shape and includes a base unit, two vertical columns and a fixed upper transverse beam, as well as a crosshead which can move up and down. The crosshead contains a load cell with maximum capacity of 300kN. The tests on RSF joints have been performed in AUT's Structures lab.

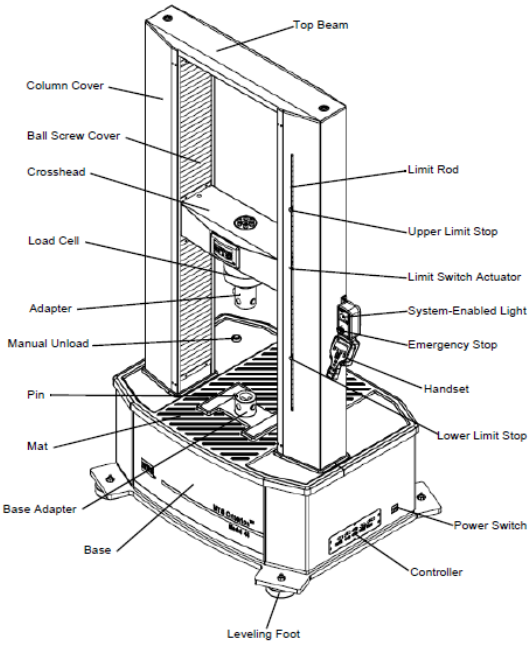

Fig 5-7. UTM system

Fig 5-8. RSF joint test setup

Fig 5-9. RSF joint at the initial position before slip

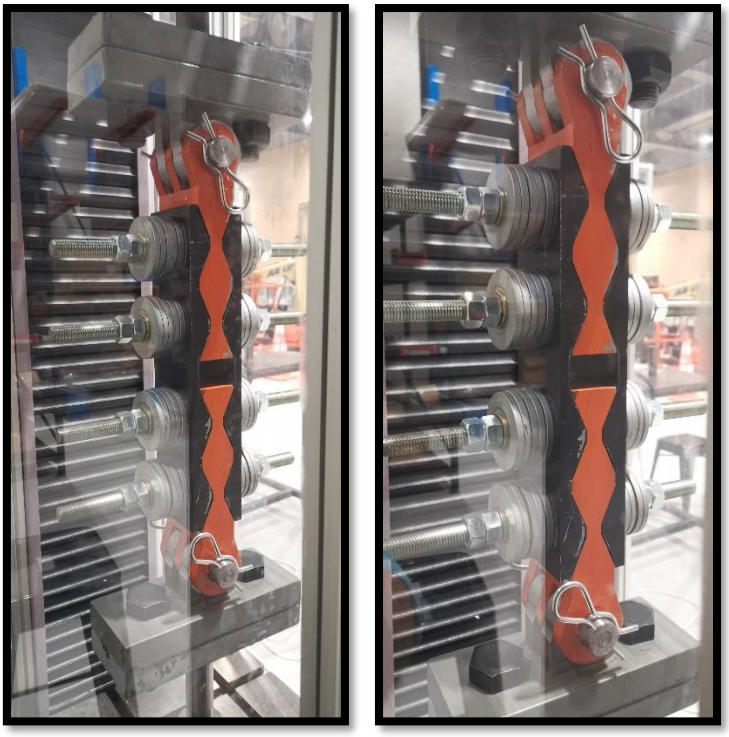

Fig 5-10. RSF joint after slip in tension

The test was performed to compare the analytical and experimental hysteresis curves of the joints. Three cycles with the amplitude of 12 mm were defined for the UTM. The loading was set as displacement controlled with a rate of 0.1 mm per second. The test has been conducted successfully. The UTM provided the results of each test as a text file. Later, the results were transferred to an Excel file to plot the load-slip curves for comparison. In Figure 5-11, the comparison between the experimental and analytical results has been illustrated.

As it can be found, the experimental hysteresis curve is compatible with the analytical predictions as per section 5-1. Both curves show a flag-shaped behaviour in RSF joints as expected. This means the joints could successfully dissipate the seismic energy during an earthquake without experiencing any damage in their components. Also, it shows the fully self-centring behaviour of the joints resulting in no residual drift in the structures.

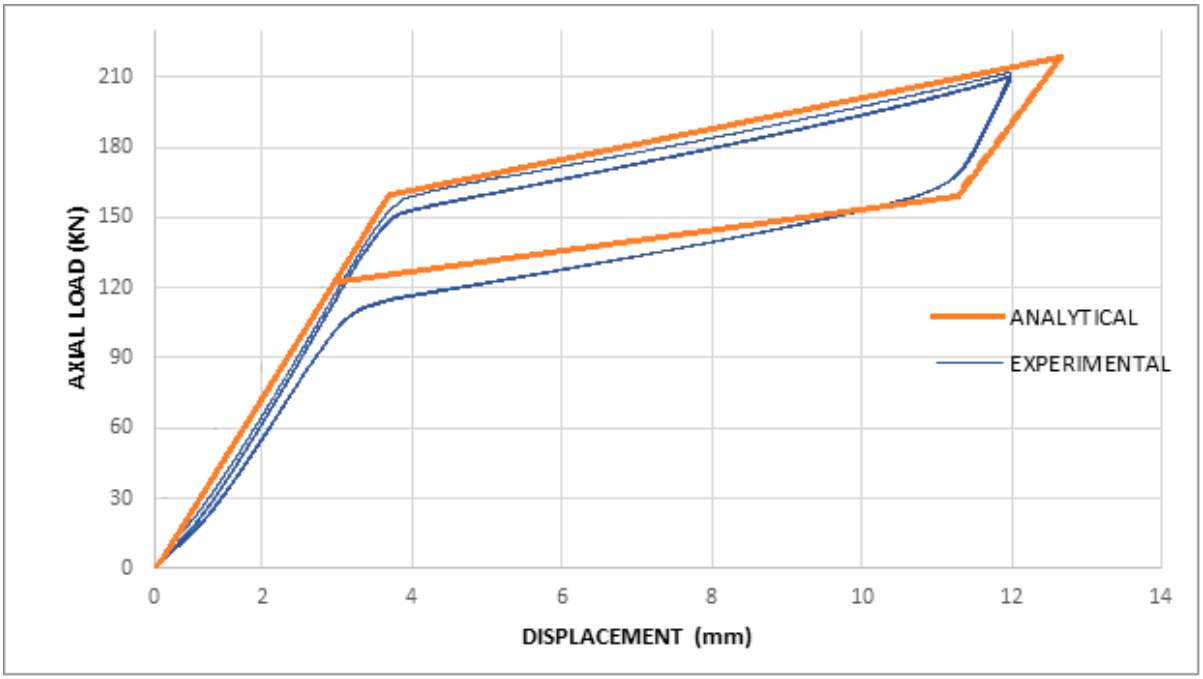

Fig 5-11. Comparison of analytical and experimental flag-shaped responses of RSF joints

6. Experimental study of a full-scale beam-end self-centring slip friction connection

In order to verify the performance of the moment connection with the RSFJs, a full-scale beam-end prototype connection test was planned. The RSFJs have been designed for the ultimate load of 220 KN. The beam and connection have been designed based on New Zealand steel structures standard (NZS 3404). It should be noted that by increasing the number of bolts (in RSFJ) or the length of the lever arm through a deeper beam, a larger capacity could be achieved for the moment connection.

6.1. Connection configuration

The general configuration of the damage avoidance steel beam moment connection with the RSFJs is demonstrated in Figure 6-1. The specimen is a 2 m cantilever beam with a universal standard section of 530UB92. The moment connection includes a purely pinned hinge which is located along the beam top flange and two RSFJs along the beam bottom flange. The pin used at the top can transfer the axial loads as well as the shear forces without affecting the rotational stiffness of the connection system.

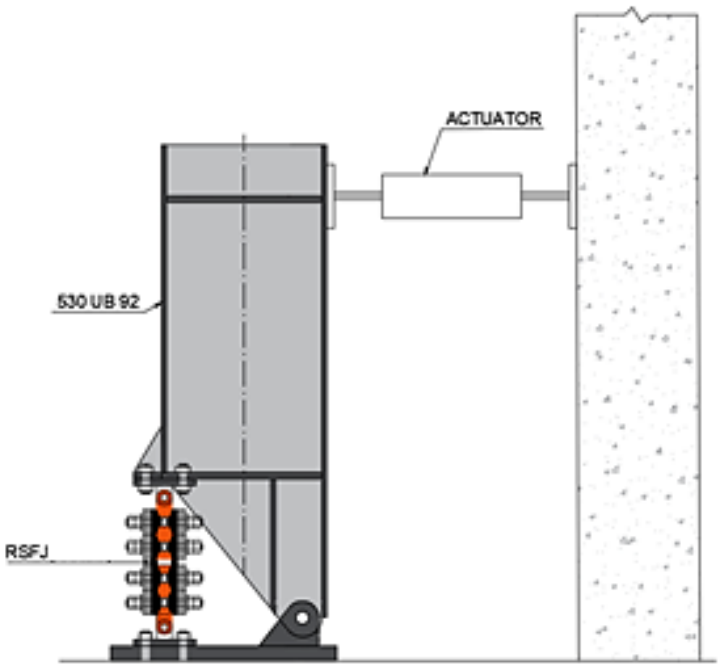

Fig 6-1. Damage avoidance steel beam moment connection with RSFJs

6.2. Connection moment-rotation response

Following the analytical spring model described in Chapter 4, the slip moment for either negative or positive moment can be determined, as follows.

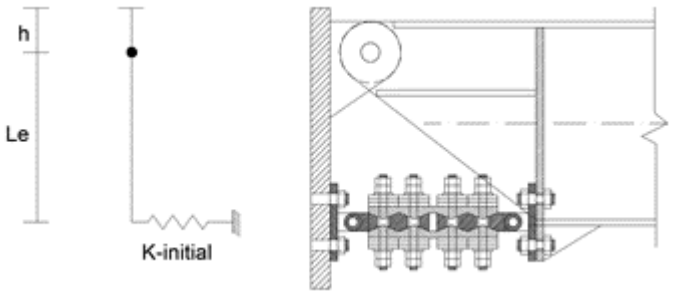

$$M_{slip} = F_{slip} \times L_e = \left(K_{initial} \times L_e \times \theta_{slip}\right) \times L_e = (K_{initial} \times L_e^2) \times \theta_{slip} = K_{\theta,initial} \times \theta_{slip}$$

$$M_{slip} = F_{slip} \times L_e = \ 160 \ \times 0.45 = 72 \ kN.m$$

$$2 \ \times RSFJ \ then : M_{slip} = 144 \ kN.m$$

After the sliding, the moment capacity of the connection increases because of the compaction of the disc springs creating additional axial resistance in the RSFJs. The connection will be at its maximum moment capacity, M_{ult} (stage 2) when the RSFJs reach their ultimate capacity $F_{RSFJ,ult.}$

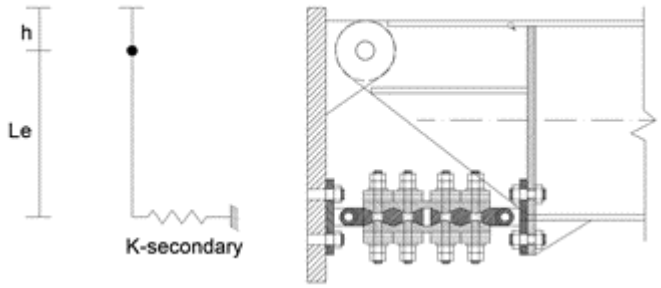

$M_{ult} = M_{slip} + M_{ult-slip}$

$M_{ult-slip} = F_{ult-slip} \times L_e = \left(K_{secondary} \times L_e \times \theta_{ult-slip}\right) \times L_e \quad = \left(K_{secondary} \times L_e^2\right) \times \theta_{ult-slip}$

$M_{ult-slip} = F_{ult-slip} \times L_e = 60 \times 0.45 = 27\ kN.m$

2 x RSFJ then: $M_{ult\text{-}slip} = 54\ kN.m$

$M_{ult} = M_{slip} + M_{ult\text{-}slip} = 144 + 54 = 198\ kN.m$

The rotation of the connection at the slip and ultimate moment ($\theta_{slip}\ and\ \theta_{ult}$) can be derived by:

$\theta_{slip} = M_{slip} / (K_{initial} \times L_e^2) = \frac{72}{43000 \times 0.45^2} = \ 0.008\ Rad$ (0.8% rotation)

$\theta_{ult} = \theta_{slip} + \theta_{ult-slip} = (0.008 + 0.02) = \quad 0.028\ Rad$

$\theta_{ult-slip} = M_{\text{ult-slip}} / \left(K_{secondary} \times L_e^2\right) = 27 / (6630 \times 0.45^2) = \quad 0.02\ Rad$ (2% rotation)

The analytical prediction of the moment-rotation response of the connection is shown in Figure 6-2.

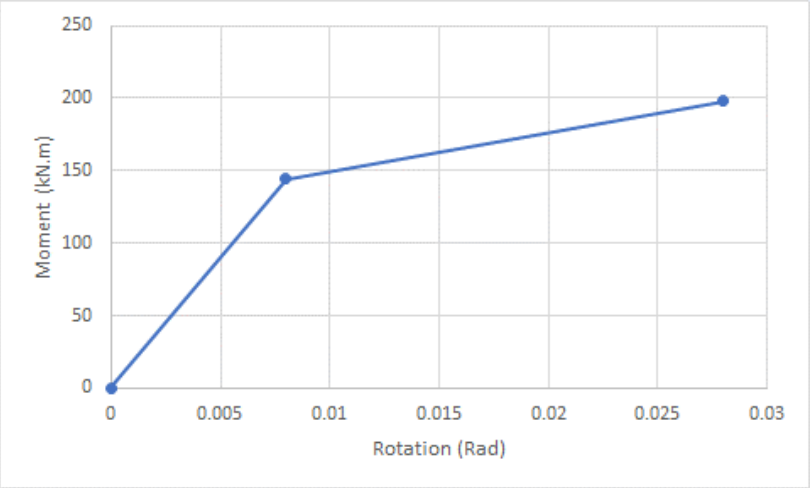

Fig 6-2. Prediction of connection moment-rotation response

6.3. Components design

In this section, the design checks of the beam and each component of the moment connection have been provided.

6.3.1. Beam section

The demand moment capacity in the beam considering the RSFJs ultimate force of 440kN (= 2*220), with a lever arm of 0.45m and an over strength factor of 1.5 was 297kN.m (= 440*0.45*1.5). Given the section bending capacity of the 530UB92 of 561 kN.m ($ØM_n = Z.f_y$, Z_{33} = 2078799.25 mm^3, f_y = 300 MPa, Ø = 0.90), the demand-capacity ratio (DCR) was 0.53, so a conservative approach.

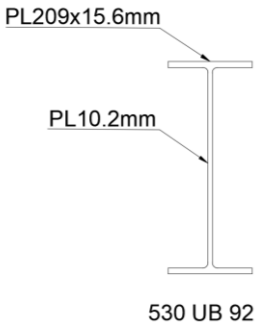

Fig. 6-3. Beam cross section

6.3.2. Beam bottom flange at the connection with RSFJs

In this section, the beam bottom flange is controlled under the maximum tension and compression forces resulting from negative and positive moments, respectively.

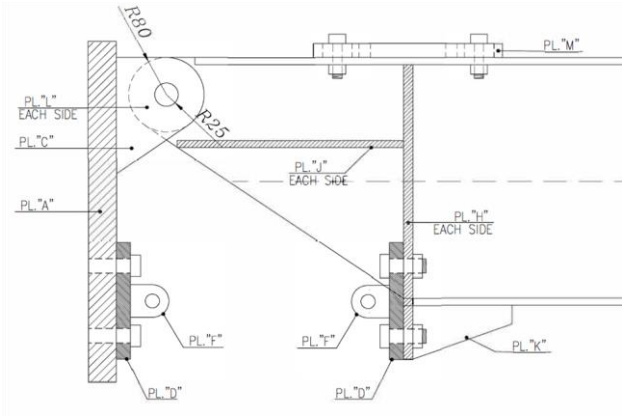

Fig 6-4. Connection of the beam with RSFJs to base plate

Tension strength check

$$\emptyset N = 0.9 \times A_s \times f_y = 0.9 \times (209 \times 15.6) \times 300 = 880\ KN > 660\ kN$$

(= 1.5× Mult / Le = 1.5×198/0.45)

Compression strength check

Checking the yielding slenderness limit:

$$\lambda e = \frac{b}{t} \times \sqrt{\frac{f_y}{250}} = \frac{250}{15.6} \times \sqrt{\frac{300}{250}} = 14.6 < 16$$ (HR: Hot rolled)

So, yielding will happen before buckling.

$$\emptyset N_s = 0.9 \times K_f \times A_s \times f_y = 0.9 \times 1 \times (209 \times 15.6) \times 300 = 880\ kN > 660\ kN$$

6.3.3. Top pin

In this section, the top pin is designed based on the maximum axial load combined with shear.

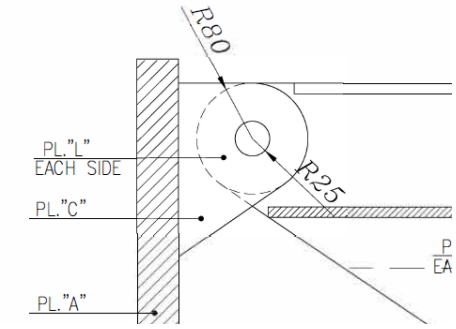

Fig 6-5. Purely pinned connection of the beam to the base plate

Shear strength control of the pin

$$\emptyset V_f = 0.9 \times 0.62 \times K_r \times f_{uf} (n_n A_c + n_x A_0)$$

$$\emptyset V_f = 0.9 \times 0.62 \times 1 \times (0.8 \times 830) \times (A_p \times 0.8 \times 2)$$

$$A_p > 660/590 = 1.136\ m^2 = 1136\ mm^2$$

For the adopted M50 G8.8 pin, the $A_p = 1962\ mm^2 > 1136\ mm^2$

Moment capacity check of the pin

The spacing between the two tabs of the base plate is 55 mm (Fig. 6-4). Conservatively, 660 kN point load has been considered at the middle of the pin, resulting in a bending demand of 4606 kN.mm (M*=PL/8).

$$\emptyset M_n = 0.9 \times Z \times f_y = 0.9 \times 12271 \times (0.8 \times 830) = 7333\ kN.mm > 4146\ kN.mm$$

6.3.4. Weld design of the tabs

In this section, welding of the tabs in pinned connection has been checked.

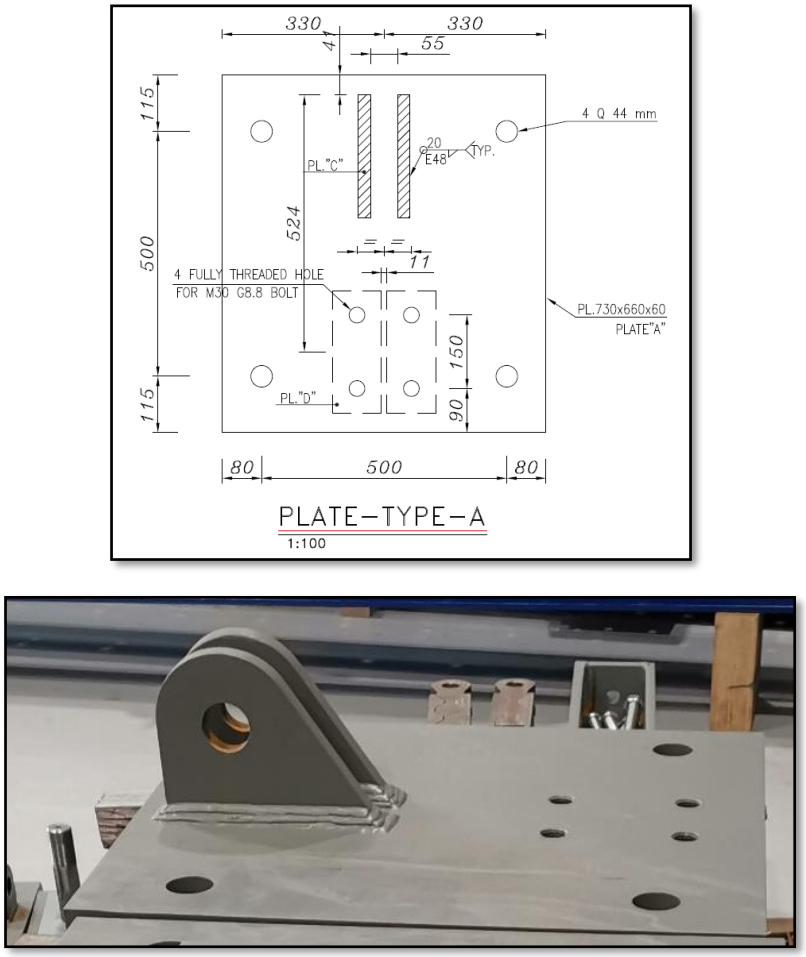

Fig 6-6. Welding of the pin bracket tabs

Shear strength check of the weld

$$ØV_w = 0.6 \times t_w \times K_r \times f_{uw} \times L$$

$$ØV_w = 0.6 \times (0.707 \times 20) \times 0.62 \times 480 \times (2 \times 250) \times 2$$

$$ØV_w = 2500\ KN > 670\ KN$$

Bending capacity of the weld

Spacing between the load and the neutral axis, *Le = 250/2-80 = 45 mm*

M = 670 × 45 = 30150 KN.mm*

For each line of welding: *M* = 30150/4 = 7537 kN.mm*

Maximum stress in the weld: $\sigma = \frac{MC}{I} = 7537000 \times \frac{125}{18411458} = 51.2\ MPa < 480\ MPa$

Shear strength check of the plate

$\emptyset V_p = 0.9 \times 0.6 \times A_s \times f_y = 0.9 \times 0.6 \times (250 \times 25) \times 300 = 1012\ KN > 660\ KN$

Checking the end distance

For checking the end distance, the bearing in controlled at the top plate of the beam (Figure 6-5).

$V^* < C_1 . \emptyset V_b$

C1=1, Ø= 0.9

$V_b = a_e . t_p . f_{up} = 0.9 \text{ x } 80 \text{ x } 50 \text{ x } 300 = 1080\ KN$

Checking shear in the main beam web

V* = M*/Le (distance between the actuator and the connection) = 297/2 = 150 KN

Shear in the thick part (with the doubler plates)

$\emptyset V = 0.9 \times 0.6 \times A_s \times f_y = 0.9 \times 0.6 \times (55 \times 50) \times 300 = 445\ KN > 150\ KN$

Fig 6-7. Doubler plates on the beam web at the pin connection

Shear in the thin part (the beam web)

$$ØV_p = 0.9 \times 0.6 \times A_s \times f_y = 0.9 \times 0.6 \times (250 \times 10.2) \times 300 = 413\ KN > 150\ KN$$

6.4. Test setup preparation and installation

After designing the beam, connection and the RSF joints, the following steps have been followed in preparation for the testing.

6.4.1. Preparation of the shop drawings

After completion of the components design, the shop drawing of each part has been prepared detailing the dimensions and specifications, as shown in Figure 6-8.

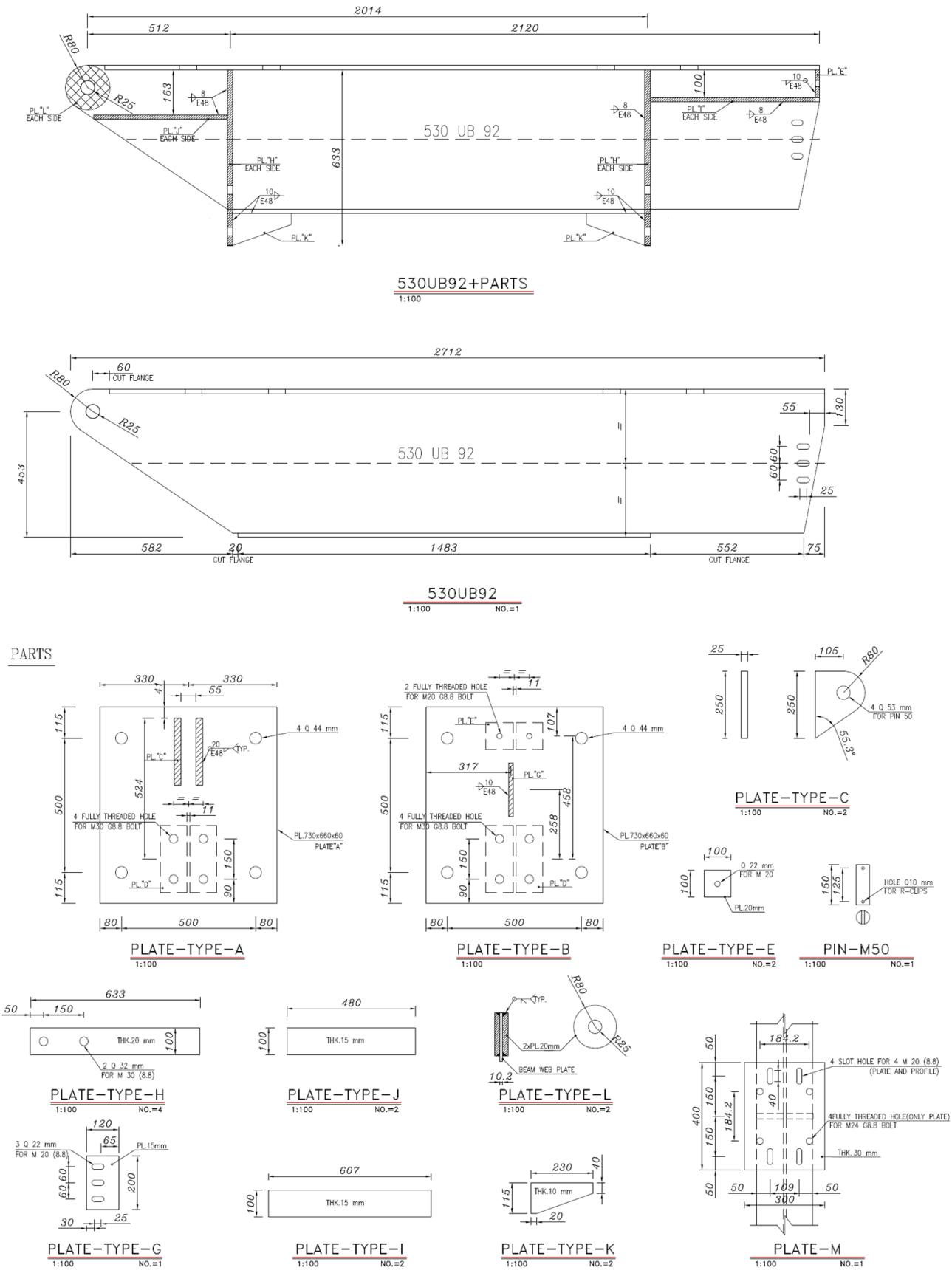

Fig 6-8. Shop drawings of the beam and the connection components

6.4.2. Manufacturing of the test setup

After preparing the shop drawings, they have been sent to several manufacturers to enquire about the lead time and the manufacturing cost involving the cutting and welding works. The manufactured parts have been shipped to AUT's Structures lab and were quality controlled before the installation.

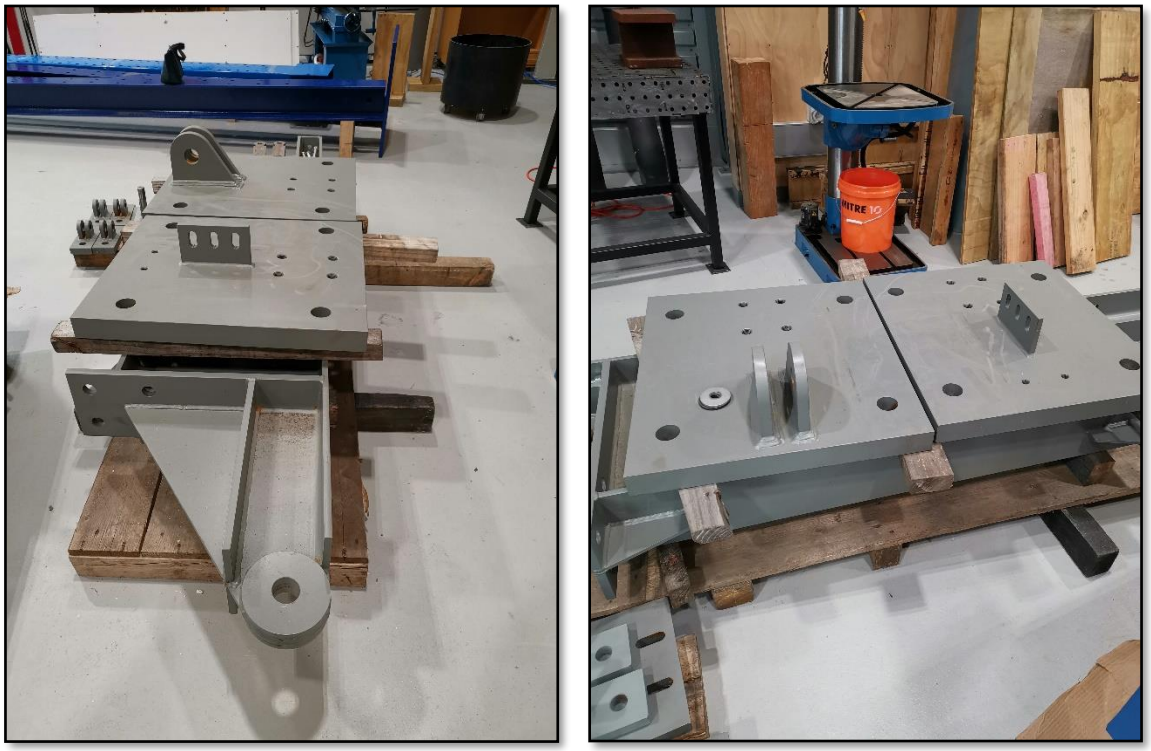

Fig 6-9. Manufactured components of the test setup

6.4.3. Test setup assembly

In this step, the position of the beam, safety frame and the actuator needed to be specified on the strong floor and the strong wall. The safety frame was considered to control the beam out-of-plane movement and prevent any potential torsion.

It was important to find the appropriate spacing between the beam and the strong wall given the limit on the stroke length of the actuator. The actuator is a hydraulically powered machine that can extend or retract (double-acting) to load the specimen or the structure attached to it. It

could be either displacement or force controlled. The oil pressure required for the operation of the actuators is provided by a Hydraulic Power Unit (HPU). The actuator includes an LVDT which measures its displacement during loading. For this test, a 250kN actuator with +/-125mm stroke capacity was used which was installed on the strong wall at one end and the other end was connected to the beam for applying the load.

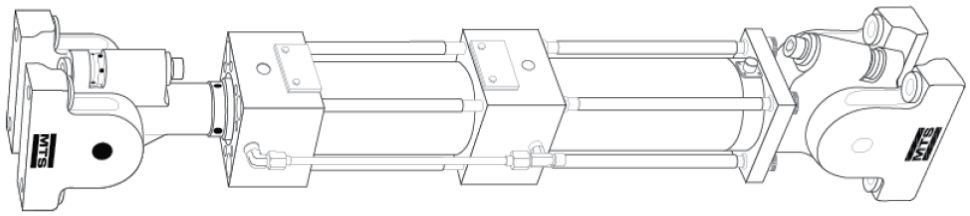

(a)

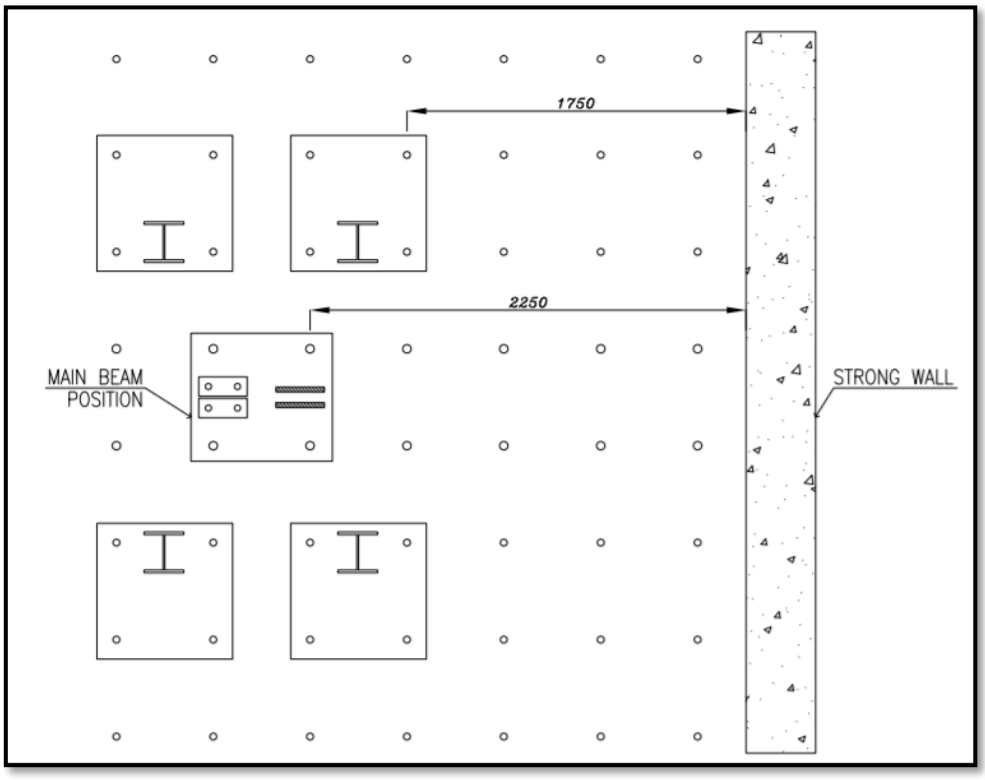

(b)

Fig 6-10. A schematic photo of actuator with swivel base (Top), Position of the beam and safety columns on the strong floor (Bottom)

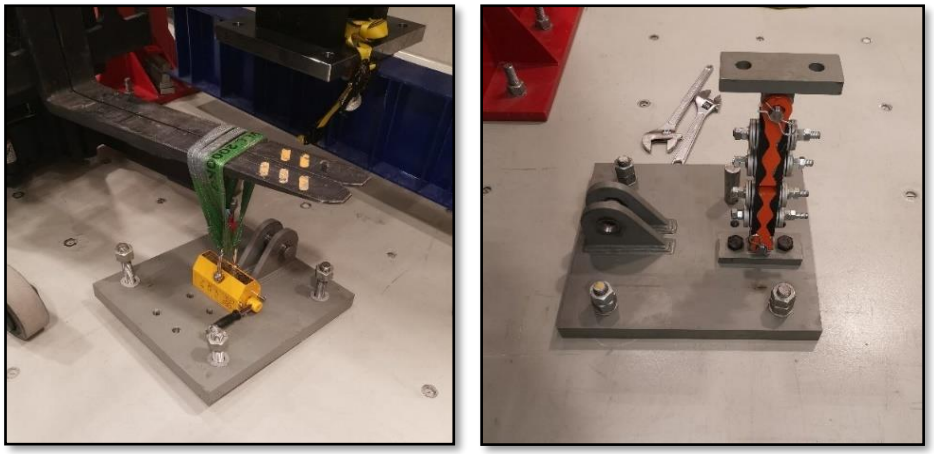

Fig 6-11. Installation of the base plate and RSFJs on the strong floor

Fig 6-12: Installing the beam and safety frames in AUT's lab

6.4.4. Installation of instruments

A drew wire has been installed on top of the cantilever beam along the actuator for recording the horizontal displacement of the beam. Also, LVDT sensors have been installed along the RSFJs for recording the axial displacement of the joints.

Fig 6-13. Installation of drew wire sensor

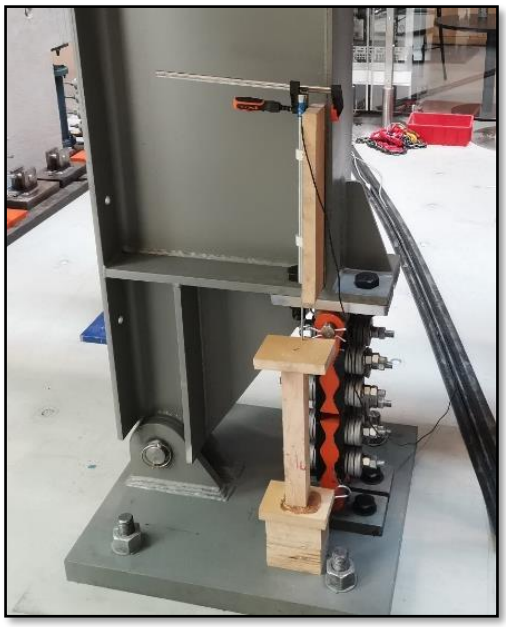

Fig 6-14. Installation of LVDT sensors

6.5. Test results and discussion

After completion of the setup, the quasi-static test has been performed to investigate the behaviour and hysteresis response of the beam connection with RSF joints. The loading protocol defined for the 250 kN actuator was following a sequence of target displacements at 15mm, 30mm, 50mm and 65mm with three cycles at each amplitude. The loading rate was set at 10 mm per second, comparable to a frequency of 0.04 Hz. The test successfully has been carried out.

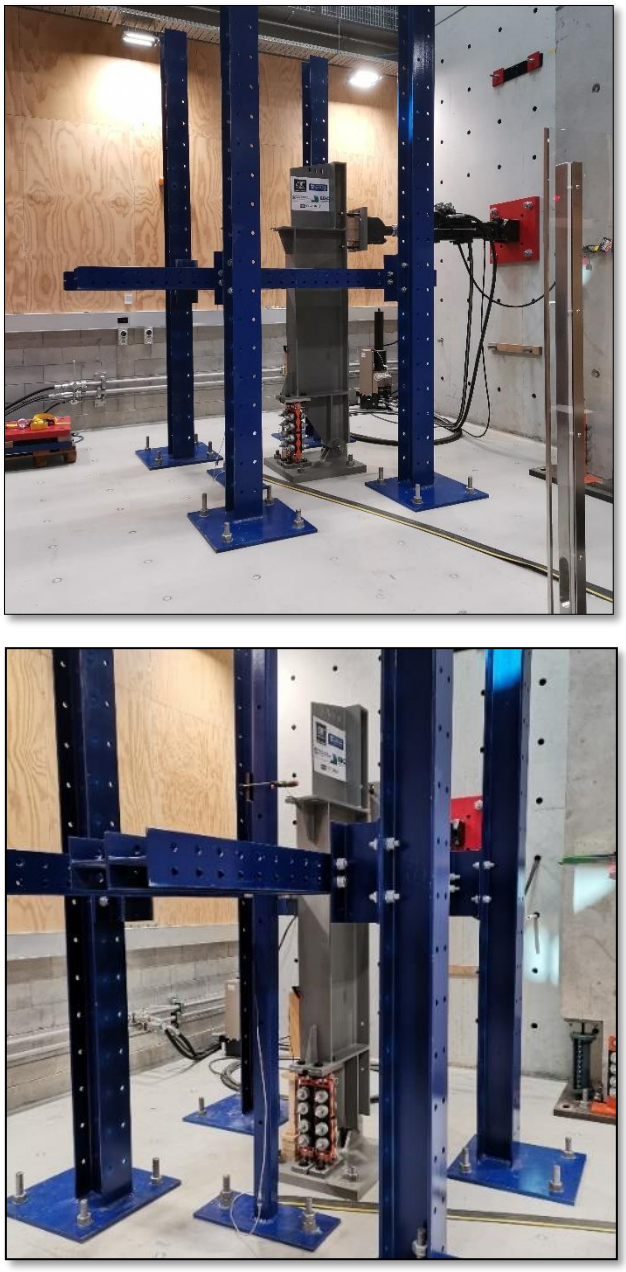

Fig 6-15. Large-scale beam connection test setup

In Figures 6-16, 6-17 and 6-18, the experimental results are shown. The first graph is the results from the LVDT sensors which indicates the axial displacement in the RSFJ. The second graph is the results from the drew wire which shows the actuator horizontal movement at top of the beam.

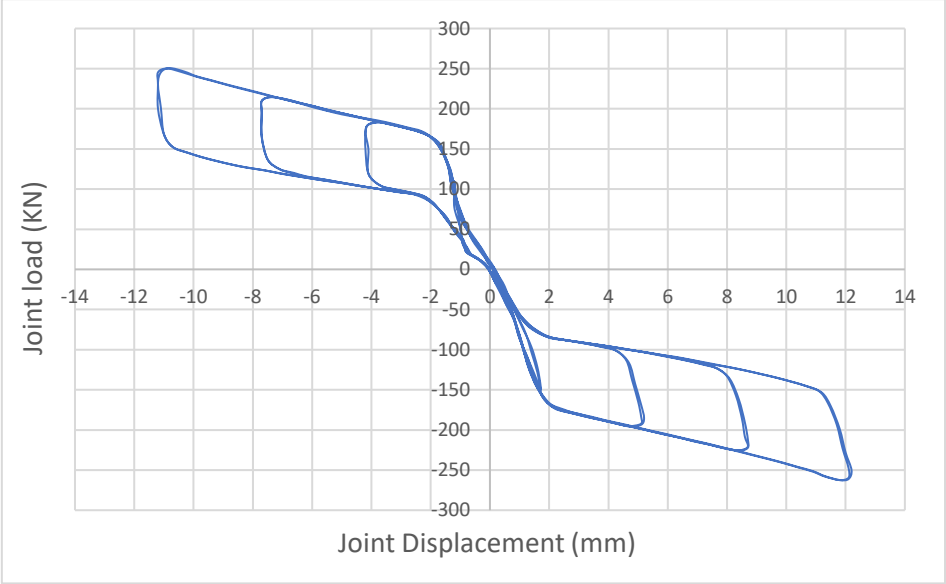

Fig 6-16. RSFJ hysteresis curves- LVDT results

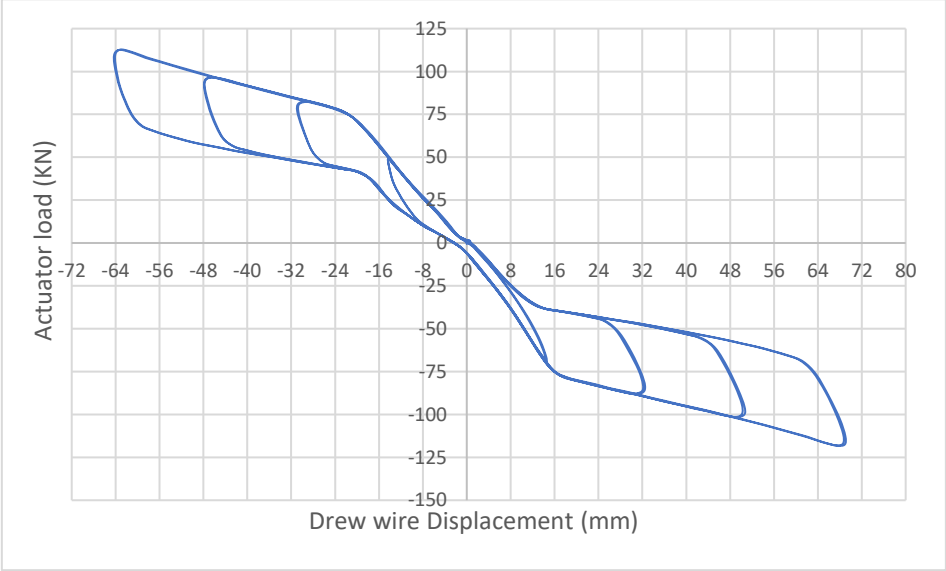

Fig 6-17. Beam hysteresis curves - Drew wire results

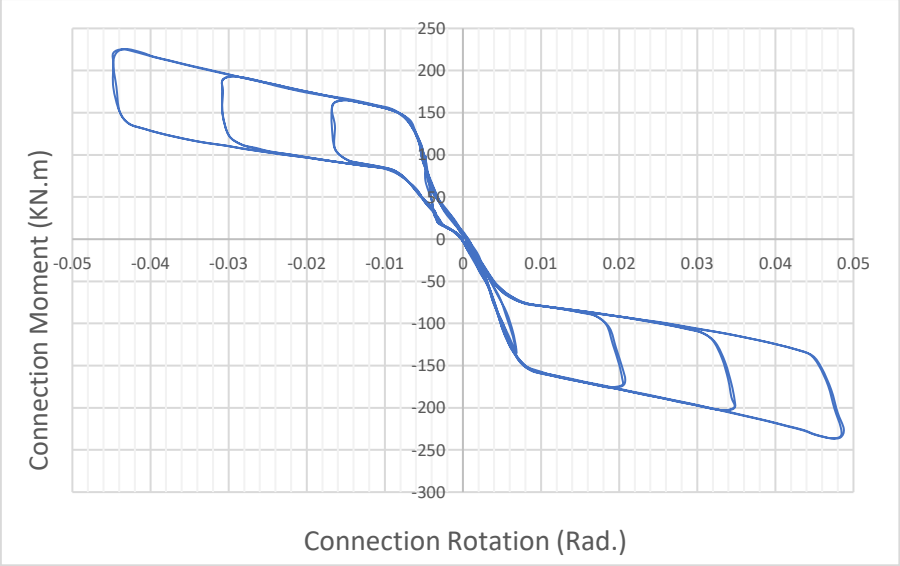

Fig 6-18. Connection hysteresis curves

The third graph, the experimental flag-shaped hysteresis behaviour in the beam moment connection which is in line with the predictions as per section 6.2. This demonstrates that the joints can efficiently dissipate the seismic energy during an earthquake without appearance of damage in the beam, connection and the joints. Also, it shows the fully self-centring behaviour of the moment connection.

7. Summary and Conclusion

Moment-resisting frames are one of the efficient lateral-load resisting systems in terms of providing architectural freedom in design and imposing smaller forces on foundation. Recent major earthquakes have resulted in significant plastic deformations in the beam-column connections causing irrecoverable damages in structures. As a result, engineers have focused on developing new systems which not only provide the life-safety of the residents, but also minimise the damage such that the building could be reoccupied quickly after severe events with minimal business interruption and repair costs.

Seismic structural systems can be classified into two categories. The first category could refer to high damage structural design solutions such as the conventional steel moment resisting frames. In this category, fully restrained welded or bolted connections have been used between the beams and columns. Conventional moment frames are designed to dissipate the energy under the design earthquake by yielding in the main structural members. That is why the structure is meant to experience damage to prevent the collapse. The yielding in the plastic hinges can lead to significant inelastic deformations in the beams and columns, resulting in permanent structural damage as well as residual story drifts after the earthquake.

Most modern design codes are following this first category as they are based on an estimate of the demand and yielding capacity. Since the plastic deformation generally happens, considerable repairs or replacements might be required after a major earthquake. Usually, in this method, the design provides sufficient detailing to meet the desired performance objectives and plastic deformation is transferred to the pre-defined positions such reduced beam sections. Of course, the other approach is to design the structure to be strong enough to prevent any inelastic or nonlinear behaviour in the structure, but this is generally uneconomic in terms of construction costs.

The second category refers to low damage designs in which there are sacrificial fuses to damp the seismic input energy and be replaceable after a severe event. After the Northridge earthquake, several research projects were commenced to improve new concepts for steel frames to decrease the onsite working and to avoid inelastic deformations posed by the yielding of the structural elements (Roeder et al., 2000). The application of friction-based energy dissipating devices in steel structures dates back to 1982 when Pall and his colleagues used such devices in the braced frames to absorb the seismic energy. Clifton and colleagues (2007 and 2010) introduced the Sliding Hinge Joint (SHJ) as a low damage solution alternative to the traditional steel MRFs. The SHJ permits for gap opening in the beam-column contact area and energy dissipation occurs by the sliding movement of the plates. To avoid structural damages and residual drift, post-tensioned beam-column connections for self-centring moment resisting frames (SC-MRFs) were proposed by Ricles et al. (2001). In which the gap opening in the contact zone of the beam-column connection provides the inelastic behaviour and the strands bring the self-centring.

In this thesis, a new self-centring damage avoidance moment connection using the innovative Resilient Slip Friction Joint (RSFJ) was developed for steel Moment Resisting Frames (MRFs). The RSFJ provides the self-centring behaviour as well as energy dissipation in one compact component requiring no post-event maintenance. In this concept, the beam is connected to the column using a pin assembly at top, and the RSFJs acting in tension and compression at the beam bottom. The RSFJs allow for the gap opening in the connection during loading and re-centres the system upon unloading. Also, a secondary collapse-prevention fuse within the RSFJ is considered to keep maintaining a ductile behaviour in the system in case of an event greater than the design earthquake.

Furthermore, in this thesis, the method of modelling the RSFJ in ETABS, SAP2000 and ABAQUS was detailed. It allows the designer to accurately calibrate the performance

parameters according to the requirements of the project. In ETABS/SAP2000, the RSFJ can be modelled using the “Damper – Friction Spring” link Element. The results of a conceptual 10-storey building model show a perfect flag shape behaviour of the structure. Also, the analytical models are developed to accurately predict the moment-rotation behaviour of this system.

Using RSFJs in connections of MRFs has several advantages which can be summarised as follows:

1- Concentrating all nonlinearity in RSF joints. So, all the members of the structure remain elastic during the earthquake and there is no need for structural repair.
2- Achieving damage avoidant connections.
3- Increasing the damping and ductility of the system.
4- No need to adopt the RSFJ in all the connections of the structure. The number and location of moment connections with RSFJs can be optimized. All pinned main and secondary steel beams can be designed as a composite section with concrete floor. This can decrease the size of the beams and the total structural cost effectively.

In order to experimentally investigate the hysteretic behaviour of the RSFJ, a series of joint component tests were conducted. Results showed that the RSFJ technology has a high potential for the application in seismic resistant structures, especially, when a resilient damage avoidant design is required in order to protect the structures from major seismic events and the associated aftershocks.

Finally, the seismic performance of the proposed concept was investigated by a full-scale experimental testing of a beam connection equipped with RSFJs. The RSFJs have been designed for the ultimate load of 250 KN. The beam and connection have been designed based on New Zealand steel structures standard (NZS 3404). The specimen was a 2 m cantilever

beam with an universal standard section of 530UB92. The moment connection contained, a purely pinned hinge which was located along the beam top flange and two RSFJs along the beam bottom flange. The pin used at the top could transfer the axial loads as well as the shear forces without affecting the rotational stiffness to the system.

The test results validate the predictive model and demonstrate the efficiency of this new self-centring system for seismic damage avoidance design of MRFs. Experimental hysteresis curves showed a flag shaped behaviour in the moment connection and the beam as it was expected. This indicates that the RSFJ can successfully dissipate the seismic energy during an earthquake without any damage in the beam, connection and joints as well as preventing the residual drift in the system.

8. References

Buchanan, A., Bull, D., Dhakal, R.P., MacRae, G., Palermo, A., and Pampanin, S. “Base isolation and damage-resistant technologies for improved seismic performance of buildings”. *Technical Report to the Canterbury Earthquakes Royal Commission*, Christchurch, New Zealand, 2011.

Build Magazine. “Seismic Technology Showcase”. Retrieved from http://www.buildmagazine.org.nz, 2014.

Canterbury Earthquakes Royal Commission (CERC). “Low-damage building technologies”. *ISBN: 978-0-478-39558-7*, Christchurch, New Zealand, 2012.

Constantinou, M. C., and M. D. Symans. "Experimental study of seismic response of buildings with supplemental fluid dampers". *The Structural Design of Tall Buildings* 2.2: 93-132, 1993.

Computers and structures, SAP2000. (2011), 2011 (Berkeley, CA).

Chang, S. E. and Falit-Baiamonte, A. (2002). "Disaster vulnerability of businesses in the 2001 Nisqually earthquake." *Environmental Hazards*, 4(2-3): 59-71.

Chou, C.-C. and Chen, J.-H. (2011). "Development of floor slab for steel post-tensioned self-centering moment frames." *Journal of Constructional Steel Research*, 67(10): 1621-1635.

Christopoulos, C., Filiatrault, A., Uang, C.-M. and Folz, B. (2002). "Posttensioned energy dissipating connections for moment-resisting steel frames." *Journal of Structural Engineering*, 128(9): 1111-1120.

Clifton, G. C. (2005). “Semi-rigid joints for moment-resisting steel framed seismic-resisting systems.” Department of Civil and Environmental Engineering, University of Auckland, Auckland.

Comerio, M. C. (2006). "Estimating downtime in loss modelling." *Earthquake Spectra*, 22(2): 349-365.

Danner, M. and Clifton, C. (1995). “Development of moment-resisting steel frames incorporating semi-rigid elastic joints.” Report R4-87. Heavy Engineering Research Association, Manukau City, New Zealand.

Filiatrault, A., Tremblay, R. and Kar, R. (2000). "Performance evaluation of friction spring seismic damper." *Journal of Structural Engineering*, 126(4): 491-499.

Garlock, M. and Li, J. (2008). "Steel self-centering moment frames with collector beam floor diaphragms." *Journal of Constructional Steel Research*, 64(5): 526-538.

Garlock, M., Ricles, J. M. and Sause, R. (2005). "Experimental studies of full-scale posttensioned steel connections." *Journal of Structural Engineering*, 131(3): 438-448.

Gledhill, S. M., Sidwell, G. K. and Bell, D. K. (2008). "The damage avoidance design of tall steel frame buildings - Fairlie Terrace Student Accommodation Project, Victoria University of Wellington." 2008 *NZSEE Conference*, Taupo, New Zealand.

Grigorian, C. E. and Popov E. P. (1994). "Energy dissipation with slotted bolted connections." Report No. UCB/EERC-74/02. Earthquake Engineering Research Centre, Berkeley, California.

Grigorian, C. E., Yang, T. S. and Popov, E. P. (1993). "Slotted Bolted Connection energy dissipators." *Earthquake Spectra*, 9(3): 491-504.

Gilton C., Chi B., Uang C.-M., "Weak-Axis and Deep Column Steel RBS Moment Connections," SSRP2000/03.

Hashemi, A., Masoudnia, R. & Quenneville, P. 2016. A numerical study of coupled timber walls with slip friction damping devices, *Constr. Build. Mater.*, Vol 121 373–385.

Hashemi, A., Masoudnia, R. & Quenneville, P. 2016. Seismic performance of hybrid self-centring steel-timber rocking core walls with slip friction connections, *J. Constr. Steel Res.*, Vol 126 201–213. *Key Engineering Materials*, Vol 763 733.

Hashemi, A., Loo, W.Y., Masoudnia, R., Zarnani, P. & Quenneville, P. 2016. Ductile Cross Laminated Timber (CLT) Platform Structures with Passive Damping, *World Conference of Timber Engineering WCTE2016*, Vienna, Austria.

Hashemi, A., Zarnani, P., Masoudnia, R. & Quenneville, P. 2017. Seismic resistant rocking coupled walls with innovative Resilient Slip Friction (RSF) joints, *J. Constr. Steel Res.*, Vol 129 215–226.

Hashemi, A., Zarnani, P., Masoudnia, R. & Quenneville, P. 2017. Seismic resilient lateral load resisting system for timber structures, *Constr. Build. Mater.*, Vol 149 432–443.

Hashemi, A., Zarnani, P., Masoudnia, R. & Quenneville, P. 2017. Experimental testing of rocking Cross Laminated Timber (CLT) walls with Resilient Slip Friction (RSF) joints, *J. Struct. Eng.*, Vol 144(1) 4017180-1-16.

Hibbitt, K. 2014. *ABAQUS*. Standard User's Manual. V. 6.13

Horwich, G. (2000). "Economic lessons of the Kobe Earthquake." *Economic Development and Cultural Change,* 48(3): 521-542.

Iyama, J., Seo, C. Y., Ricles, J. M. and Sause, R. (2009). "Self-centering MRFs with bottom flange friction devices under earthquake loading." *Journal of Constructional Steel Research,* 65(2): 314-325.

Kim, H.-J. and Christopoulos, C. (2008). "Friction damped posttensioned self-centering steel moment-resisting frames." *Journal of Structural Engineering,* 134(11): 1768-1779.

King, A. (2007). "Design of collector elements for self-centering moment resisting frames." Master of Science in Civil Engineering, Purdue University.

MacRae, G. A., Clifton, C., MacKinven, H., Mago, N., Butterworth, J. and Pampanin, S. (2010)."The Sliding Hinge Joint moment connection." *Bulletin of the New Zealand Society for Earthquake Engineering,* 43(3): 202-212.

Midstate Precast. "Concrete solution for high-performance buildings". Retrieved from http://cenews.com/article/8918/concrete-solution-for-high-performance-buildings, 2012.

New Zealand Treasury (2012). "Budget Economic and Fiscal Update 2012."

Priestley, M. J. N. and MacRae G. A. (1996). "Seismic tests of precast beam-to-column joint subassemblages with unbonded tendons." *PCI Journal,* 41(1): 64-80.

Ramhormozian S., Clifton G. C., MacRae G. A., "The Asymmetric Friction Connection with Belleville springs in the Sliding Hinge Joint", 2014 *NZSEE Conference*, New Zealand

Ramhormozian S., Khoo H., Clifton C., MacRae G., Zhou H., Proposed design models for the asymmetric friction connection, Earthq. Eng. Struct. Dyn. 44 (2015) 1309–1324

Ricles, J. M., Sause, R., Garlock M. and Zhao, C. (2001). "Post-tensioned seismic-resistant connections for steel frames." *Journal of Structural Engineering,* 127(2): 113-121.

Ringfeder Gmbh (2008). Damping Technology. Catalogue R60. Krefeld, Germany.

Roeder, C. W. (2002). "Connection performance for seismic design of steel moment frames." *Journal of Structural Engineering*, 128(4): 517-525.

Rodgers, G. W., Chase, J. G., Mander, J. B., Dhakal, R. P., & Solberg, K. M. "DAD Post-Tensioned Concrete Connections with Lead Dampers: Analytical Models and Experimental Validation". *8th Pacific Conference on Earthquake Engineering*, 2007.

Sato A., Newell J., Uang C.-M., "Cyclic Testing of Bolted Flange Plate Steel Moment Connections for Special Moment Frames", SSRP-07/10.

Sumner E.A., Mays T. W., and Murray T. M., "End-plate moment connections: test results and finite element method validation", 4th International workshop, 2000.

Simpson Strong-Tie company INC, "Strong Frame- Design Guide", 2017.

Standards New Zealand (2004). *NZS 1170.5 - Structural design actions. Earthquake actions*. Wellington, New Zealand.

Standards New Zealand (2009). *NZS 3404 - Steel structures standard*. Wellington, New Zealand.

Tierney, K. J. (1997). "Business impacts of the Northridge Earthquake." *Journal of Contingencies and Crisis Management*, 5(2): 87-97.

Wolski, M., Ricles, M. J. and Sause, R. (2009). "Experimental study of a self-centering beam-column connection with bottom flange friction device." *Journal of Structural Engineering*, 135(5): 479-488.

Yang, T.-S. and Popov, E. P. (1995). "Experimental and analytical studies of steel connections and energy dissipators." Report No. UCB/eerc-95/13. Earthquake Engineering Research Center, Berkeley, University of California.

Yeh, C.-H., Loh, C.-H. and Tsai, K.-C. (2006). "Overview of Taiwan Earthquake loss estimation system." *Natural Hazards*, 37(1): 23-37.

Zarnani, P. & Quenneville, P. 2015. *A resilient slip friction joint*, Patent No. WO2016185432A1, NZ IP Office.

Zarnani, P., Valadbeigi, A. & Quenneville, P. 2016. Resilient slip friction (RSF) joint: A novel connection system for seismic damage avoidance design of timber structures, *World Conf. on Timber Engineering WCTE2016*, Vienna Univ. of Technology, Vienna, Austria.